Electroweak phase transition and LHC signatures in the singlet Majoron model

James M. Cline,[a] **Guillaume Laporte,**[a] **Hiroki Yamashita**[a,1] **and Sabine Kraml**[b]

[a]*McGill University, Department of Physics,*
Montréal, Québec H3A 2T8, Canada

[b]*Laboratoire de Physique Subatomique et de Cosmologie, UJF Grenoble 1, CNRS/IN2P3, INPG,*
53 Avenue des Martyrs, F-38026 Grenoble, France

E-mail: jcline@physics.mcgill.ca, guillaume.laporte@mail.mcgill.ca,
sabine.kraml@lpsc.in2p3.fr

ABSTRACT: We reconsider the strength of the electroweak phase transition in the singlet Majoron extension of the Standard Model, with a low ($\lesssim$ TeV) scale of the singlet VEV. A strongly first order phase transition, of interest for electroweak baryogenesis, is found in sizeable regions of the parameter space, especially when the cross-coupling $\lambda_{\rm hs}|S|^2|H|^2$ between the singlet and the doublet Higgs is significant. Large Majorana Yukawa couplings of the singlet neutrinos, $y_i S\nu_i^c\nu_i$, are also important for strengthening the transition. We incorporate the LEP and Tevatron constraints on the Higgs masses, and electroweak precision constraints, in our search for allowed parameters; successful examples include singlet masses ranging from 5 GeV to several TeV. Models with a strong phase transition typically predict a nonstandard Higgs with mass in the range 113 GeV $\lesssim m_H \lesssim$ 200 GeV and production cross sections reduced by mixing with the singlet, with $\cos^2\theta$ significantly less than 1. We also find examples where the singlet is light and the decay $H \to SS$ can modify the Higgs branching ratios relative to Standard Model expectations.

---

[1]Current address: Barclays Capital Japan Limited.

Contents

1 Introduction

Nonstandard Higgs sectors are interesting from the perspective of LHC physics and cosmology. While the Standard Model predicts a smooth cross-over for the electroweak phase transition (EWPT) [1], extensions can give a strongly first-order phase transition, which is a necessary ingredient for electroweak baryogenesis, and could also possibly generate observably large gravitational waves [2] or primordial magnetic fields [3]. Supersymmetric extensions of the Standard Model have been studied the most intensively in this respect [4], but it is also possible to get a strong transition from more generic two-Higgs doublet models [5, 6], from technicolor theories [7], higher-dimension operators involving the Standard Model Higgs [8], or from singlets which mix with the Standard Model Higgs [9–17]. In the last category, the singlet Majoron model [18] is an interesting example since it was originally motivated by the spontaneously breaking of lepton symmetry and consequent

generation of neutrino masses by the seesaw mechanism. It is the model which we consider in the present work.

In the singlet Majoron model, right-handed neutrinos $\nu_{R,i}$ acquire Majorana masses $M_i = y_i\langle S \rangle$ through their Yukawa couplings to the complex singlet field S, when it gets a VEV. Denoting the Yukawa couplings to the doublet Higgs by $h_i\bar{\nu}_{L,i}H\nu_{R,i}$, the seesaw masses of the light neutrinos are given by

$$m_{\nu,i} = \frac{h_i^2 v^2}{y_i\langle S \rangle} \tag{1.1}$$

where v is the VEV of H. If the Yukawa couplings are $O(1)$, then $\langle S \rangle \sim v^2/m_{\nu,i}$, a very high scale $\gtrsim 10^{14}\,\mathrm{GeV}$. This is the usual assumption, which would render the singlet field irrelevant for physics at the electroweak scale. However, we know that small Yukawa couplings exist even in the Standard Model: that of the electron is $O(10^{-6})$. If the h_i are also of this order (while $y_i \sim 1$), then $\langle S \rangle$ could be as small as $10^{-12}v^2/(0.1\text{ eV}) \sim 300\,\mathrm{GeV}$. From this point of view, a low scale for the singlet is no less natural than the Standard Model itself, and merits consideration.

The effect of the singlet Majoron on the EWPT has been considered previously in [17], but these papers were written before the final LEP/Tevatron bounds on the Higgs boson mass m_H or values of electroweak precision observables (EWPO) were known, and thus they could not take these important constraints into account.[1] As is well appreciated, the strength of the EWPT tends to be inversely related to m_H; moreover the EWPO constraints tend to exclude heavy singlet fields which have significant mixing with the Higgs doublet. There have also been studies of related models [10–16], where the singlet is a real field, or a complex one such that the global U(1) symmetry under which S might transform is explicitly broken by terms like S^3. These models are also very interesting, but sufficiently different from the Majoron model to justify a separate study of the latter. The models with explicitly broken symmetry are more generic, but not motivated by considerations of neutrino physics. Moreover, cubic terms in the scalar potential tend to make it easier to find a first-order phase transition, so we would expect the physics leading to a strong EWPT to be qualitatively different in the two classes of models. Indeed we will show that the coupling of the right-handed neutrinos to S plays an important role in getting a strong phase transition in the Majoron model.

Because the global lepton symmetry is spontaneously broken, the imaginary part of S is a Goldstone boson, the Majoron. Since we are assuming the doublet Yukawa couplings to be quite small ($h_i \lesssim O(10^{-6})$), the massless Majoron couples very weakly to the light neutrinos, with strength $h_i v/\langle S \rangle$. These couplings are diagonal in the mass basis at this order; off-diagonal couplings which could lead to neutrino decays are suppressed by $(h_i v/\langle S \rangle)^2$ (see ref. [19] and references therein). Such a weakly coupled Majoron goes out of equilibrium well before nucleosynthesis, and also has a negligible effect on energy loss from stars, and so it is experimentally unconstrained.[2]

---

[1]It is possible to evade the EWPO constraints, so we will present results both with and without applying them.

[2]In contrast to the scenarios discussed in ref. [15], we do not require the singlet to provide a dark matter candidate.

In the remainder of the paper, we derive the finite-temperature effective potential (section 2), and present our methods and results for the strength of the EWPT from a wide search of the model's parameter space (section 3). We analyze the nonstandard decay modes and discovery potential of the singlet sector at the LHC in section 4. Conclusions are given in section 5. We present formulas for field-dependent and thermal masses needed for the potential in the appendices, as well as those pertaining to our renormalization prescription, the running of the couplings, and formulas for the oblique parameters for electroweak precision observables.

2 The potential

Because the left-handed neutrino Yukawa couplings are assumed to be very small for our purposes, we neglect them in what follows. Similarly, only the top quark is retained amongst the other fermions of the Standard Model. At tree level the potential is then

$$V_0 = \lambda_h \left(|H|^2 - \frac{1}{2} v_h^2 \right)^2 + \lambda_s \left(|S|^2 - \frac{1}{2} v_s^2 \right)^2 + \lambda_{\rm hs} |S|^2 |H|^2 + y_t \bar{Q} H t_r + \frac{1}{2} \sum_i y_i S \nu_i \nu_i + {\rm h.c.}$$

(2.1)

in terms of the complex Higgs doublet $H = (H^0, H^+)$, complex singlet S, top quark and right-handed neutrinos. For definiteness, we take three generations of right-handed neutrinos with equal Majorana Yukawa couplings y_i. Due to the cross-coupling $\lambda_{\rm hs}$, v_h and v_s are not generally the VEV's of the fields at the minimum of the potential. Rather, the relation is

$$v_s^2 = 2\langle S \rangle^2 + \frac{\lambda_{\rm hs}}{\lambda_s} \langle H \rangle^2;$$

$$v_h^2 = 2\langle H \rangle^2 + \frac{\lambda_{\rm hs}}{\lambda_h} \langle S \rangle^2;$$

(2.2)

We take $\langle H \rangle \cong 174\,{\rm GeV}$ and $\langle S \rangle$ (to be varied) as the physical input parameters. Because of the Z_2 symmetries $H \to -H$ and $S \to -S$ in the scalar potential, there is no loss in generality in assuming that both VEV's are positive. (The signs of the fermion masses are not physically significant.)

At finite temperature, the lowest order thermal correction to V_0 is a function of the field-dependent particle masses, $m_i(H, S)$:

$$\Delta V_T = T \sum_i \pm \int \frac{d^3 p}{(2\pi)^3} \ln \left(1 \mp e^{-\beta \sqrt{p^2 + m_i^2(H,S)}} \right) \begin{cases} {\rm bosons} \\ {\rm fermions} \end{cases}$$

(2.3)

where $\beta = 1/T$. These functions are often approximated by their high temperature expansions, but for numerical purposes it is preferable to use an approximation that works at all values of m_i/T. We use the approximation described in ref. [5], in which the high-T and low-T expansions are smoothly joined together at some large value of m_i/T. This is reviewed in appendix A. The expressions for the field-dependent thermal masses are given in appendix B.

– 3 –

Furthermore, it is important to improve the thermal contribution by resumming the ring diagrams, which amounts to replacing m_i^2 with the thermally corrected masses (of the form $m_i^2 + c_i T^2$) in eqs. (2.3). Otherwise there is a danger of overestimating the strength of a first order phase transition. Often, this substitution is made only in the cubic term of the high-T expansion, where it has the biggest effect on the barrier between the true and false vacua of the potential [20]. However, when one uses an expression that correctly captures both the large and the small m_i/T behavior of (2.3), there is no way to consistently include thermal mass effects only in the cubic term, since it appears explicitly only in the high-T expansion. Trying to do so creates a kink in the potential when the high-T and low-T expansions are joined onto each other. To avoid such complications, we simply replace m_i^2 by its thermally corrected value everywhere in (2.3) [21]. The discrepancy between the two approaches is formally significant only when computing the potential to two loops.

The thermal potential (2.3) can be regarded as a one-loop effect, so for consistency one must also include the one-loop, zero-temperature (Coleman-Weinberg) correction to the potential,

$$\Delta V_{\rm CW} = \frac{1}{2}A|H|^2 + \frac{1}{64\pi^2}\sum_i m_i^4(H,S)\left(\ln\frac{m_i^2(H,S)}{\mu^2} - \frac{3}{2}\right) \times \begin{cases} +1, \text{ bosons} \\ -1, \text{ fermions} \end{cases} \quad (2.4)$$

where $A|H|^2$ is a counterterm and μ is the renormalization scale. We do not include a counterterm of the form $B|S|^2$ because this can be absorbed into a redefinition of v_s. However for the doublet Higgs it is convenient to introduce the $A|H|^2$ counterterm, because then one can maintain the tree-level relation between the Higgs VEV $\langle H \rangle$ and v_h. In fact, it is convenient to maintain both relations (2.2), so that the position of the zero-temperature minimum of the potential $H = \langle H \rangle$, $S = \langle S \rangle$, is known analytically. We thus adopt as our renormalization prescription

$$\frac{\partial V}{\partial H} = \frac{\partial V}{\partial S} = 0 \qquad \text{at} \qquad H = \langle H \rangle, \quad S = \langle S \rangle \quad (2.5)$$

where $V = V_0 + \Delta V_{\rm CW}$. These two equations can be analytically solved to find μ and A (see appendix C).

A notable feature of $\Delta V_{\rm CW}$ is that the terms $\ln(m_i^2(H,S))$ appear in such as way as to exactly cancel corresponding terms in the high-T expansion of ΔV_T; then the cubic term $(m_i^2)^{3/2}$ of ΔV_T is the only source of nonanalytic dependence on the fields. To preserve this property, we also replace m_i^2 by the thermally corrected expression in $\Delta V_{\rm CW}$ when we do the ring improvement of the potential [21].

A complication which arises in the effective potential is the appearance of negative values of $m_i^2(H,S)$ for the Goldstone boson degrees of freedom at small H or S; this can happen even when the thermal correction to m^2 is included. Such values create a problem with the cubic term $(m_i^2)^{3/2}$ in the high-T expansion of the thermal potential. Even if one takes only the real part, which vanishes for negative m^2, derivatives of this with respect to the fields are discontinuous at the point where m^2 changes sign, leading to serious difficulties for algorithms which attempt to minimize the potential. There are various prescriptions in the literature for dealing with the Goldstone bosons. We take the simplest approach, which

is to simply omit their contributions from $\Delta V_{\rm CW}$ and ΔV_T. Experience with other models indicates that the Goldstone bosons never have a strong effect on the phase transition in any case. Thus we omit the contributions from $H^{\pm}$, $\mathrm{Im}(H^0)$, and the Majoron j in the sums.

In the limit of very heavy singlet and neutrinos, one expects the effects of the new physics to decouple. This is evident in the low-T expansion of the thermal correction to the potential, since the effects of heavy particles are Boltzmann suppressed. However, this decoupling is missing from the naive thermal corrections to the masses, (B.4)–(B.4), which were derived from the high-T expansion of the potential. To correct for this, we insert Boltzmann factors involving the heavy particle masses,

$$\delta m_H^2 = T^2 \left(\frac{1}{2}\lambda_h + \frac{1}{12}\lambda_{\rm hs}e^{-m_S/T} + \frac{1}{16}(3g^2 + g'^2) + \frac{1}{4}y_t^2 \right) \tag{2.6}$$

$$\delta m_S^2 = T^2 \left(\frac{1}{3}\lambda_s + \frac{1}{6}\lambda_{\rm hs} + \frac{1}{24}\sum_i y_i^2 e^{-m_\nu/T} \right) \tag{2.7}$$

where m_S and m_ν are evaluated at zero temperature and at the minimum of the potential. This procedure is somewhat rough, but better than ignoring the issue altogether [22].

3 Search of parameter space

Our goal was to make a broad scan of the parameter space, in search of models giving a sufficiently strong EWPT for electroweak baryogenesis. We used a $30 \times 15^2 \times 20 \times 30$ grid ($\sim 4 \times 10^6$ points) on the five parameters $\lambda_{\rm hs}$, λ_h, λ_s, y_i (taking equal Majorana Yukawa couplings for 3 generations of right-handed neutrinos) and $\langle s \rangle$, the VEV of the real component of S, $\langle s \rangle = \sqrt{2}\langle S \rangle$. After a preliminary scan of the parameter space to determine the values of interest, these were taken to be in the ranges

$$0 < \lambda_s, \lambda_h < 3, \qquad -3 < \lambda_{\rm hs} < 3, \qquad 0 < y_i^2 < 8, \qquad \langle s \rangle < 1800 \text{ GeV} \tag{3.1}$$

subject to the constraint $\lambda_{\rm hs} > -\sqrt{\lambda_h \lambda_s}$ which is needed for V to be bounded from below for large field values (at tree level). The chosen ranges include large values of the coupling constants, but since $\lambda_i^2/4\pi, y_i^2/4\pi \lesssim 1$, they are not unreasonably large.

We find that the typical pattern of symmetry breaking is to first develop a finite-temperature VEV at $S = S_{c1}$ for S alone as T is lowered from very high values, i.e., the phase transition for the singlet to condense usually occurs above the EWPT. The electroweak transition is a jump from this false vacuum along the S axis to a true vacuum in which $H \neq 0$; furthermore $\langle S \rangle = S_{c2}$ increases relative to its value in the $\langle H \rangle = 0$ minimum if $\lambda_{\rm hs} < 0$, and decreases if $\lambda_{\rm hs} > 0$. This pattern is shown in figure 1. Although S_{c1} is typically large, we will see that it can sometimes (when $\lambda_{\rm hs} < 0$) be zero.

When $|\lambda_{\rm hs}| < 1$, the mixing between the H and S fields is small, and the transition takes place mostly in the H direction. For larger values of $|\lambda_{\rm hs}|$, which are more typical of cases with a strong EWPT, the induced H-S mixing causes the tunneling path to be along a linear combination of the fields. This is illustrated in figure 2. It is easy to understand the shapes of the valleys in the potential indicated in figures 1, 2. First, the discrete
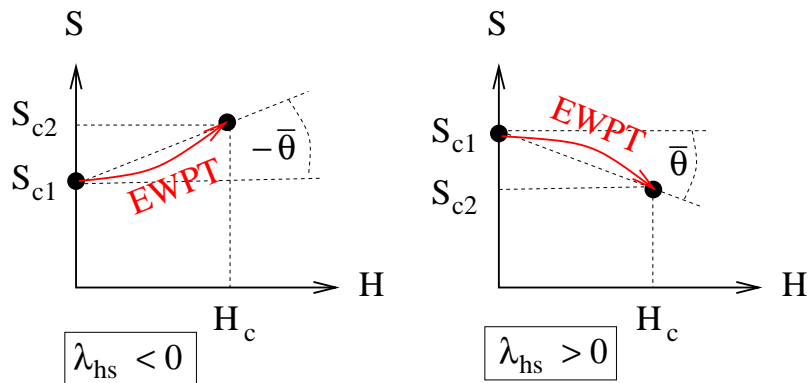
Figure 1. Trajectories of typical EWPT in H-S field space. The significance of the mixing angle $\bar{\theta}$ is discussed near eq. (3.9).
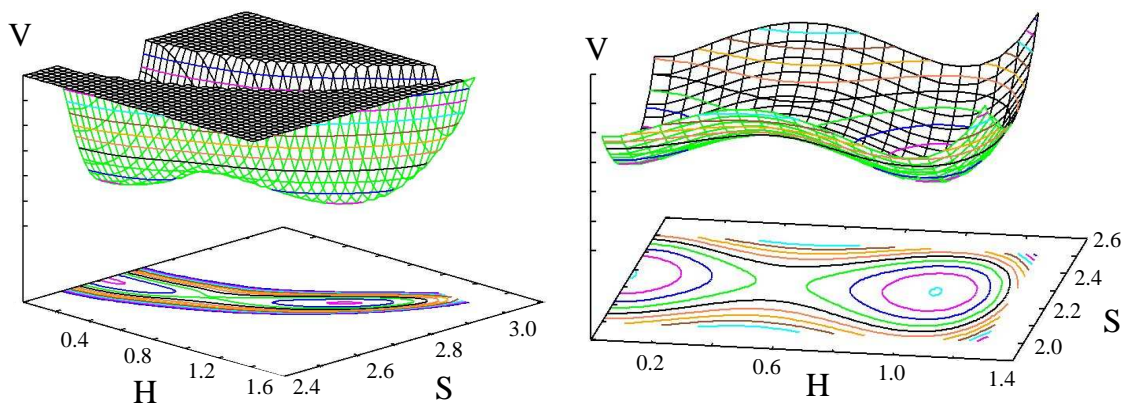

Figure 2. Shape of potential $V(H, S)$ at the critical temperature for large value of $\lambda_{\rm hs} = -2.4$ (left) and small value $\lambda_{\rm hs} = -0.2$ (right), illustrating the effect of $\lambda_{\rm hs}$ on the path in field space between the degenerate minima. Contours of the potential are projected onto the lower plane. H, S are in units of $100\,{\rm GeV}$.

symmetry $H \to -H$ implies that the light direction will be purely parallel to the H axis at $H = 0$. When H gets a VEV, the term $\lambda_{\rm hs}|H|^2|S|^2$ makes the squared mass of S more negative if $\lambda_{\rm hs} < 0$, increasing the VEV of S in the electroweak symmetry breaking vacuum. Conversely the VEV of S is decreased for $\lambda_{\rm hs} > 0$.

The above discussion makes it possible to understand why the mixing term $\lambda_{\rm hs}|H|^2|S|^2$ can generally strengthen the EWPT. Roughly, we expect the VEV of H to scale like the square root of $-\mu_h^2$, the negative mass squared term for H. When S has a VEV, $-\mu_h^2$ gets a contribution $\lambda_{\rm hs}\langle S \rangle^2$. Now suppose that $\langle S \rangle^2$ changes by the amount $\delta\langle S \rangle^2$ when H makes the transition between the symmetric and electroweak symmetry breaking EWSB vacua. We expect that the critical value H_c increases with $\lambda_{\rm hs}\,\delta\langle S \rangle^2$. The preceding discussion shows that this quantity is always positive, regardless of the sign of $\lambda_{\rm hs}$, so the mixing term should tend to strengthen the EWPT whenever it has a significant size.
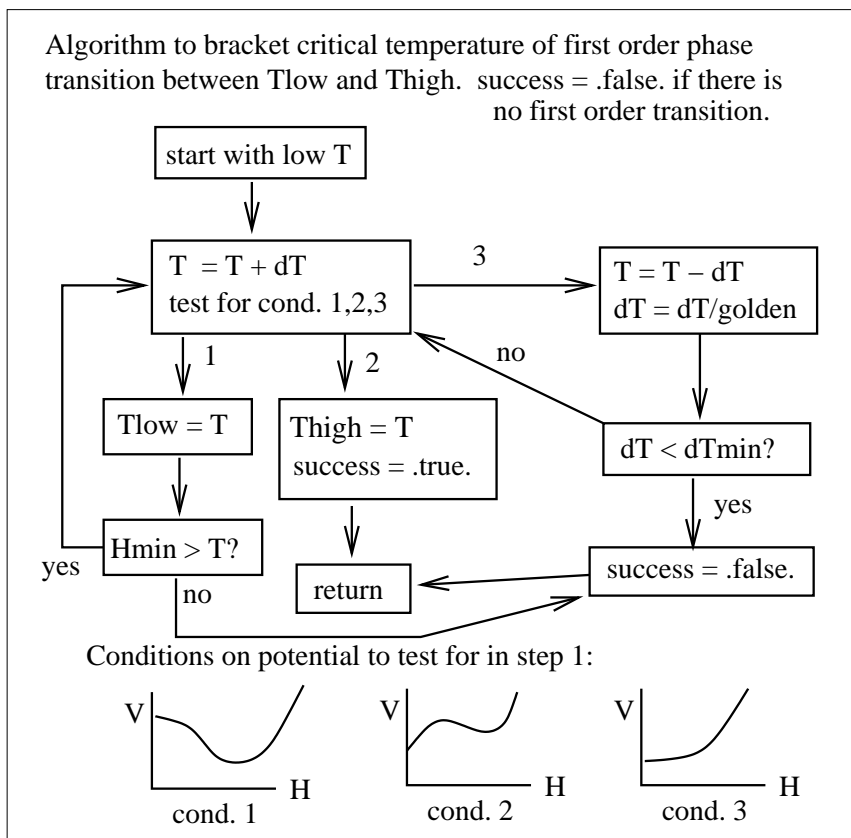
Figure 3. Flowchart for algorithm to bracket the critical temperature for a first order phase transition.

3.1 Algorithm

Because the phase transition typically proceeds in two steps, due to the two condensing fields, automating the search for a strong first order transition proved to be somewhat more difficult in this model than for effectively single-field models. The key steps are to identify whether there is a barrier between the trivial $\langle H \rangle = 0$ minimum and the EWSB $\langle H \rangle \neq 0$ minimum, and to bracket the critical temperature if there is one. Figure 3 outlines our algorithm. It outputs a logical variable success to indicate whether a first order transition with $v_c/T_c > 1$ was found, and bracketing temperatures Tmin and Tmax if so.

The algorithm shown in figure 3 is simple to implement in a single-field model, but when there are two fields it can be difficult to properly identify the relevant direction along which to check the curvature of the potential. In the present case, we start by finding the global electroweak symmetry breaking minimum near $T = 0$, and a local S-breaking minimum or saddle point on the S axis, and raise the temperature until these two critical points become degenerate. Naively, the tunneling path would be along a line connecting these two points, but because of the "banana" effect shown in figure 2, the relevant flat direction might really be curved. One must therefore determine the curvature locally around the two putative minima to check that they really are minima. If the transition

is actually second order but the transition path is curved, one could mistakenly conclude that it is first order by measuring the curvature of the potential along the straight line rather than the curved path. Of course a visual inspection of the shape of the potential would eliminate such cases, but we needed to automate this. To do so, we minimize the potential on small circles surrounding the putative local minima, to verify that they indeed are minima, and to find the directions of shallowest ascent.

3.2 Criteria for accepted points

The basic requirement for a strong enough phase transition is

$$\frac{v_c}{T_c} \gtrsim 1 \tag{3.2}$$

where v_c is the VEV of the real Higgs field h ($\sqrt{2} \times 174 \cong 246\,\text{GeV}$ at zero temperature) at the critical temperature T_c [23] (see [24] for a pedagogical review). This avoids the washout of baryons produced during the EWPT by sphalerons. A more careful treatment would be to calculate the sphaleron energy in the model at hand, since this can in principle be different from the Standard Model value and change the bound. The change is typically small however, and so we do not consider this effect.

In addition, we demand that the LEP limit on the Higgs mass [25] be satisfied. In this regard, another important feature of the $\lambda_{\text{hs}}|H^2||S^2|$ interaction is that it can cause large mixing between the singlet and doublet Higgs bosons, leading to a reduction in the production cross section for the lightest mass eigenstate [26]. We take the fluctuations of the flavor and mass eigenstates to be related via

$$\begin{pmatrix} \delta H \\ \delta S \end{pmatrix} = \begin{pmatrix} \cos\theta & \sin\theta \\ -\sin\theta & \cos\theta \end{pmatrix} \begin{pmatrix} \delta H' \\ \delta S' \end{pmatrix} \tag{3.3}$$

We restrict $\cos\theta \geq 1/\sqrt{2}$, so that H' is the "Higgs-like" state and S' is the "singlet-like" state, regardless of which one is heavier. The mixing angle suppresses the couplings of either state relative to the couplings of a SM Higgs boson. The production cross section of the Higgs-like state is reduced by $\cos^2\theta$, while that of the singlet-like state scales like $\sin^2\theta$. We demand that both of these are less than the LEP limit; i.e., both $\cos^2\theta$ and $\sin^2\theta$, evaluated at the appropriate mass, must be less than the value in column (a) of table 14 of ref. [25]. The bound is shown in figure 4. The procedure of applying the same bound independently to both states must be modified if the two are close to each other in mass. However we will find that for cases that give rise to a strong EWPT, there is always a large separation between the masses, justifying this simpler approach.[3]

Recently, the D0 and CDF experiments have disclosed new limits excluding the SM Higgs boson in the region $160 - 170\,\text{GeV}$ [27]. We fit the limit on $\cos^2(\theta)$ from table XIX in this region with the quadratic function $\cos^2\theta_{\max} = 142.43 - 1.716\,m_{H'} + 0.0052\,m_{H'}^2$

---

[3]In particular, we find no cases where both $m_{H'}$ and $m_{S'} < 114.4\,\text{GeV}$; in this situation the decays $H' \to S'S'$ or $S' \to H'H'$ (if kinematically allowed) could modify the branching ratios with respect to the Standard Model prediction.
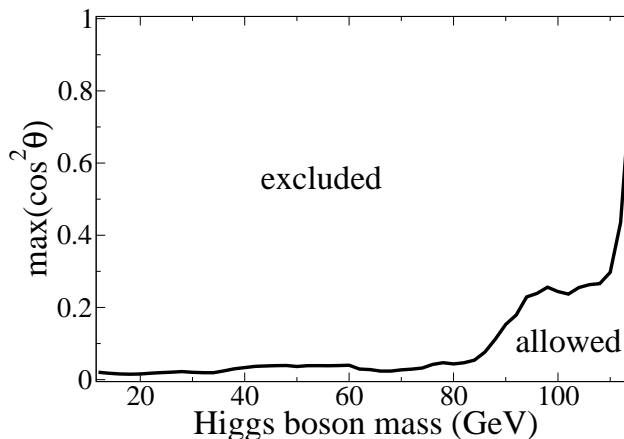
Figure 4. 95% c.l. LEP bound on mixing angle ($\cos^2\theta$) of the mostly-doublet Higgs state, from table 14 of ref. [25]. The same bound applies to $\sin^2\theta$ for the mostly-singlet state.

where $m_{H'}$ is in GeV. This has values 0.99, 0.86, 0.99 at $m_{H'} = 160, 165, 170$. Because of this limited range, the effect is small in our first search of parameter space, which involves a large range of couplings. However in the search which targets smaller couplings, the CDF/D0 limit covers a larger fraction of the range of allowed masses, and the mixing angles tend to be smaller, and so the constraint has a more pronounced effect: 450 out of 5300 parameter sets are removed.

Some cases of interest have very light singlets. Ref. [28] noted that values of $m_{S'} \lesssim 5\,\mathrm{GeV}$ (the B meson mass) are strongly constrained ($\theta < 10^{-2}$) by the decays $B \to S'X$ followed by $S' \to \mu^+\mu^-$. We thus exclude $m_{S'} \lesssim 5\,\mathrm{GeV}$ if the mixing angle is greater than 0.01. This has a negligible effect on our broader search of the parameter space since a very small fraction of this sample has light singlets, but in the search which is limited to smaller values of the coupling constants, this constraint is more significant.

Another important criterion is that the EWSB vacuum at $T = 0$ must exist. Although this seems obvious, our broad scan of parameter space includes cases where, due to radiative corrections to the tree-level Higgs potential, the curvature of the potential is positive when $H = 0$, leading to no EWSB. In fact, we will see that some concentrations of the preferred parameter space tend to be close to this perilous edge, especially when $\lambda_{\mathrm{hs}} < 0$.

Since we consider models with large couplings and large masses, a consistency requirement for perturbation theory to be under control is that none of the running couplings diverge (reaching a Landau pole) at renormalization scales smaller than the heaviest particle masses. The beta functions for the largest couplings are given in appendix D. For each otherwise accepted parameter set, we integrate these to find the first Landau pole and discard parameters which fail this test. This eliminates approximately 15% of otherwise accepted parameter sets from the range (3.1).

Finally, we include constraints on the oblique parameters S, T, U from electroweak precision observables (EWPO). In order to not to mask the intrinsic dynamics of the phase transition too much, we chose to first present results without inclusion of the EWPO constraint. A separate section 3.5 is devoted to showing how the results are affected by its inclusion. We give details about its implementation there and in appendix E.
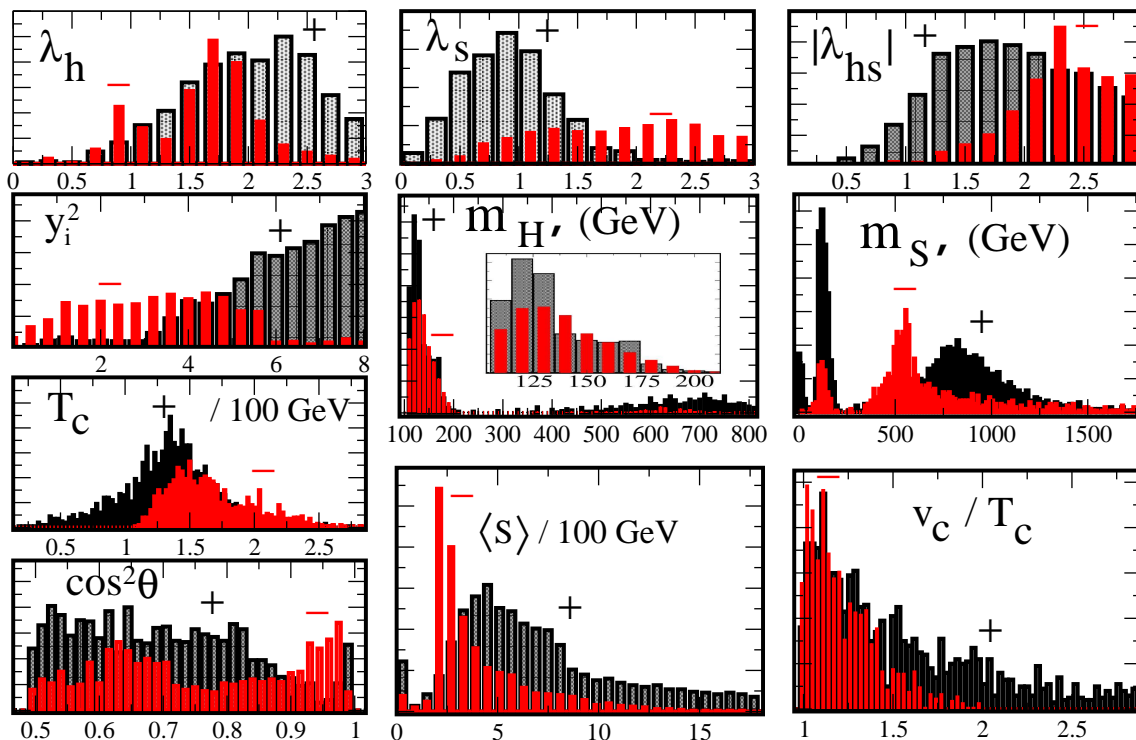
Figure 5. Distributions of parameters which generate a strong enough first order phase transition. Lighter (red) bars correspond to $\lambda_{hs} < 0$, darker (black) to $\lambda_{hs} > 0$, and $|\lambda_{hs}|$ is shown in the distribution for λ_{hs}. $\pm$ sign indicates regions associated with $\lambda_{hs} \gtrless 0$. $\langle s \rangle$ is the real (not complex) singlet VEV.

3.3 Distributions of parameters

Out of the 4×10^6 points tested on our uniform grid in the parameter space, approximately 0.07% generate a strong enough phase transition and fulfill the other criteria mentioned above. We display the distributions of accepted parameters in figure 5. The samples are divided into two groups, according to whether $\lambda_{hs} < 0$ or $\lambda_{hs} > 0$, due to the expected qualitative differences between the two cases. These differences are highlighted by the separate distributions shown for $\lambda_{hs} < 0$ and $\lambda_{hs} > 0$. One feature which they have in common however is the need for generally large values of $|\lambda_{hs}|$, in agreement with our argument that H-S mixing is important for boosting the strength of the phase transition.

Another striking feature of the distributions is the preference for large values of the Majorana neutrino Yukawa coupling, y_i^2, and the largest values being correlated with $\lambda_{hs} > 0$. It was pointed out in ref. [29] that new heavy fermions with a large Yukawa coupling to the Higgs could strengthen the EWPT. One might wonder whether this could be the origin of the need for large y_i^2 in our model, since both VEV's S and H are changing during the phase transition. However, the sign goes the wrong way. The heavy fermion effect requires the fermion to be heavier in the EWSB phase than in the symmetric phase. Figure 1 shows that this is the case when $\lambda_{hs} < 0$, but not for $\lambda_{hs} > 0$. However the preference for large y_i^2 is greater for $\lambda_{hs} > 0$ in figure 5.
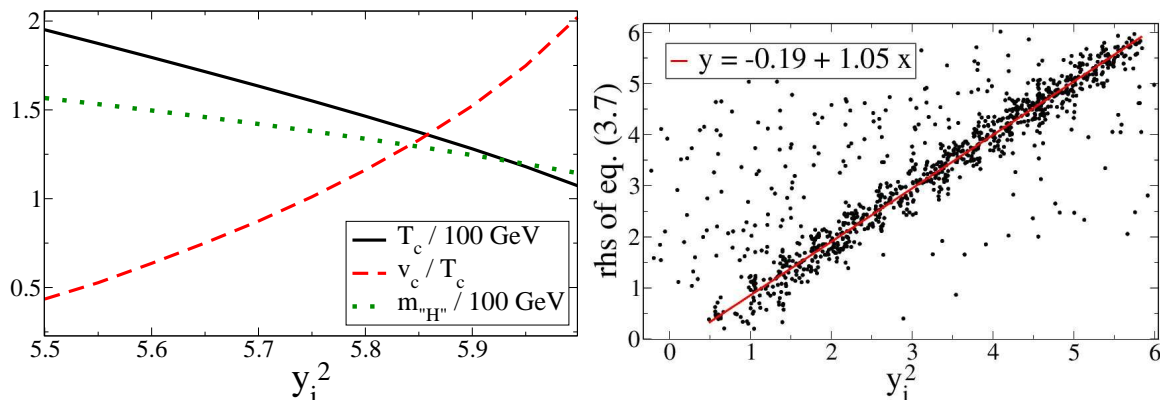
Figure 6. (a) Left: T_c, lightest Higgs mass $m_{\text{"}H\text{"}}$ and v_c/T_c as a function of y_i^2, for representative point $\lambda_{\text{hs}} = 1.90$, $\lambda_h = 1.70$, $\lambda_s = 0.90$, $\langle s \rangle = 570\,\text{GeV}$. (b) Right: the r.h.s. of eq. (3.7) versus y_i^2 for parameter sets leading to a strong EWPT. Solid line is the fit to the cluster of points which nearly satisfy this linear relation.

To understand this behavior, we have varied y_i^2 away from the accepted value for some sample points. We typically find that v_c/T_c is an increasing function of y_i^2, while the light Higgs mass is decreasing. There is thus a tension between the demand for a strong phase transition and the LEP bound, which results in a narrow window of allowed y_i^2 values, while keeping the other couplings fixed. These dependencies on y_i^2 are illustrated around a sample accepted point in figure 6(a).

By testing many hypotheses, we eventually discovered an analytic explanation for the trends visible in the distributions of parameters in figure 5. It depends crucially on the one-loop zero-temperature correction to the effective potential. Let us try to make a rough analytic estimate of the strength of the phase transition, which is characterized by v_c/T_c. The critical temperature is approximately where the temperature-dependent mass squared of H, evaluated at $(H, S) = (0, S_{c1})$, goes through zero. Using the field-dependent mass m_{hh}^2 of (B.1), the one-loop counterterm A of (2.4), and the temperature correction (B.4), we get $T_c^2 \sim (m_{\text{hh}}^2(0, S_{c1}) - A)/(\delta m_{\text{hh}}^2/T^2)$. Putting these results together gives the estimate

$$T_c \sim \frac{\sqrt{\lambda_h \langle H \rangle^2 - \lambda_{\text{hs}}(S_{c1}^2 - \langle S \rangle^2) - A}}{\sqrt{\frac{1}{2}\lambda_h + \frac{1}{12}\lambda_{\text{hs}} + \frac{1}{4}}} \tag{3.4}$$

The critical temperature can become small relative to v_c if the Higgs mass renormalization constant A, eq. (C.2), becomes large. This can happen when the renormalization scale $\ln \mu^2$, eq. (C.1), becomes large. It is straightforward to show that

$$\ln \mu^2 \sim \frac{O(\lambda_s^2, y_i^4, \lambda_{\text{hs}}^2)\langle S \rangle^2 + \lambda_{\text{hs}} O(\lambda_{\text{hs}}, \lambda_h, \lambda_s)\langle H \rangle^2}{(24\lambda_s^2 - 6y_i^4 + \lambda_{\text{hs}}^2)\langle S \rangle^2 + (\lambda_{\text{hs}}^2 + \lambda_{\text{hs}}(4\lambda_h + 6\lambda_s))\langle H \rangle^2} \tag{3.5}$$

where the numerator is correct in order of magnitude, while the denominator is exact. Since $\ln \mu^2$ appears in A, eq. (C.2), large values of $\ln \mu^2$ can cause A to be large,

$$A \sim \frac{\ln \mu^2}{16\pi^2} \left(O(\lambda_h^2, +\lambda_{\text{hs}}^2)\langle H \rangle^2 + \lambda_{\text{hs}} O(\lambda_s, \lambda_h, \lambda_{\text{hs}})\langle S \rangle^2 \right) \tag{3.6}$$
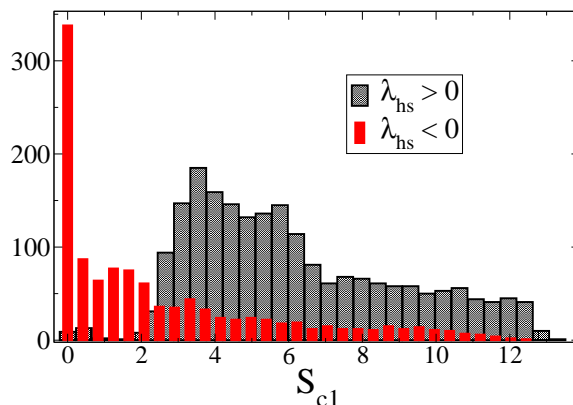
Figure 7. Distribution of S_{c1}, the scalar VEV in the electroweak symmetric vacuum at the critical temperature.

The denominator of eq. (3.5) vanishes when the relation

$$y_i^2 = \left(4\lambda_s^2 - \frac{1}{6}\lambda_{\mathrm{hs}}^2 + \frac{\langle H \rangle^2}{6\langle S \rangle^2}(\lambda_{\mathrm{hs}}^2 + 4\lambda_h \lambda_{\mathrm{hs}}) \right)^{1/2} \tag{3.7}$$

is satisfied. The correlation between y_i^2 and the r.h.s. of eq. (3.7) is shown in figure 6(b). This relation is just what one would expect from trying to minimize T_c by making $\ln \mu^2$, hence A, large. For smaller y_i^2, the strength of the transition rapidly diminishes. For larger values, we lose the EWSB vacuum because the curvature m_{hh}^2 has the wrong sign at $H = 0$.

This effect also allows us to understand other features of the distributions shown in figure 5. Eq. (3.7) shows that when $\lambda_{\mathrm{hs}} > 0$, larger values of y_i^2 result due to the term $4\lambda_h \lambda_{\mathrm{hs}}$; this trend is seen in the histogram for y_i^2. Similarly, this term puts a limit on the magnitude of λ_h when $\lambda_{\mathrm{hs}} < 0$ but not when $\lambda_{\mathrm{hs}} > 0$, in agreement with the histogram for λ_h. Moreover, inverting the relation (3.7) to express λ_s in terms of the other variables readily explains why larger values of λ_s are favored for $\lambda_{\mathrm{hs}} < 0$. Solving for $\langle H \rangle^2 / \langle S \rangle^2$ similarly shows why larger values of $\langle S \rangle$ occur for $\lambda_{\mathrm{hs}} > 0$. In short, the relation (3.7) allows us to qualitatively understand most of the trends exhibited in figure 5. The Coleman-Weinberg potential thus plays an important role in strengthening the EWPT. We have further tested this conclusion by running our program with the one-loop zero-temperature correction turned off, finding that the number of accepted points is drastically reduced in this case.

We mentioned earlier that the VEV of S in the electroweak symmetric vacuum, S_{c1}, can also be zero, but only when $\lambda_{\mathrm{hs}} < 0$. The distribution of S_{c1} in figure 7 indeed shows a spike at $S_{c1} = 0$ for $\lambda_{\mathrm{hs}} < 0$. Figure 1 makes it clear why there such is a correlation between S_{c1} and λ_{hs}: for $\lambda_{\mathrm{hs}} > 0$, S must decrease during the transition. It cannot do so if it is already zero. Eq. (3.4) also gives insight into this correlation: large values of S_{c1} are disfavored when $\lambda_{\mathrm{hs}} < 0$ since this tends to increase T_c and decrease v_c/T_c.
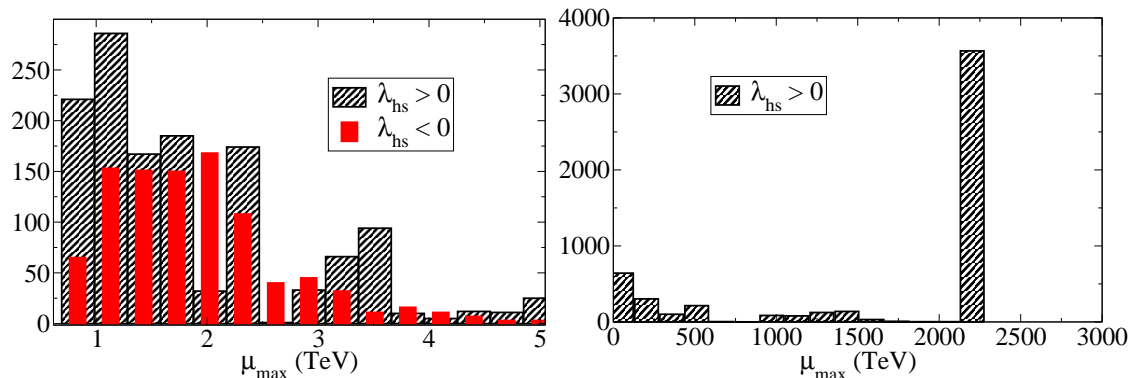
Figure 8. Distributions of maximum renormalization scale, where Landau pole develops, for the large-coupling parameter sets (left panel) and the smaller-coupling ones (right panel).

3.4 Regime of smaller couplings

It is interesting to know how important it is to have large coupling constants to get a significant effect on the EWPT. With such large couplings as the maximum values used in the scan described above, one expects to reach a Landau pole in one of the couplings at a relatively low renormalization scale $\mu_{\max}$. We have investigated this by integrating the renormalization group equations for λ_h, λ_s, $\lambda_{\rm hs}$, y_i and y_t (appendix D). The distributions of $\mu_{\max}$ plotted in figure 8 show that indeed new physics beyond the singlet and the right-handed neutrinos must typically come in at the scale of several TeV. (This would also be true in any model which uses the mechanism of ref. [29], since strong couplings are always needed to get that effect.)

This motivated us to further explore the model at somewhat weaker interaction strengths. We thus made an additional scan of the same point density as described previously, but in the more limited range

$$0 < \lambda_s, \lambda_h < 1, \qquad -1 < \lambda_{\rm hs} < 1, \qquad 0 < y_i^2 < 2, \qquad \langle s \rangle < 1800 \,\text{GeV} \qquad (3.8)$$

Encouragingly, none of the accepted parameters from this range fail the Landau pole test, showing that indeed perturbation theory is more reliable in this case. (In fact $\mu_{\max}$ is always greater than 50 TeV for this sample.) We find that almost no points are accepted for $\lambda_{\rm hs} < 0$, nor for $\langle s \rangle > 100 \,\text{GeV}$, but there is a sizeable number of accepted parameters with $\lambda_{\rm hs} > 0$ and $\langle s \rangle < 50 \,\text{GeV}$. These points have small mixing angles, $\sin^2 \theta \lesssim 0.02$ (due to the LEP constraint), and small singlet masses, $m_S \lesssim 20 \,\text{GeV}$. Their phase transitions tend to follow a circular arc in the H-S plane, between the H and S axes, as shown in figure 9(a). A curious feature is that S_{c1} and S_{c2} are typically an order of magnitude larger than the small zero-temperature VEV $\langle S \rangle$, due to $\langle H \rangle$ and hence the mixing being different at high temperature relative to $T = 0$. The parameter distributions are shown in figure 10. Unlike in the broader region of parameter space described in the previous section, here we do not find any correlation like that in eq. (3.7); thus these points give rise to a strong phase transition for different reasons than the majority of those in the large coupling regime.
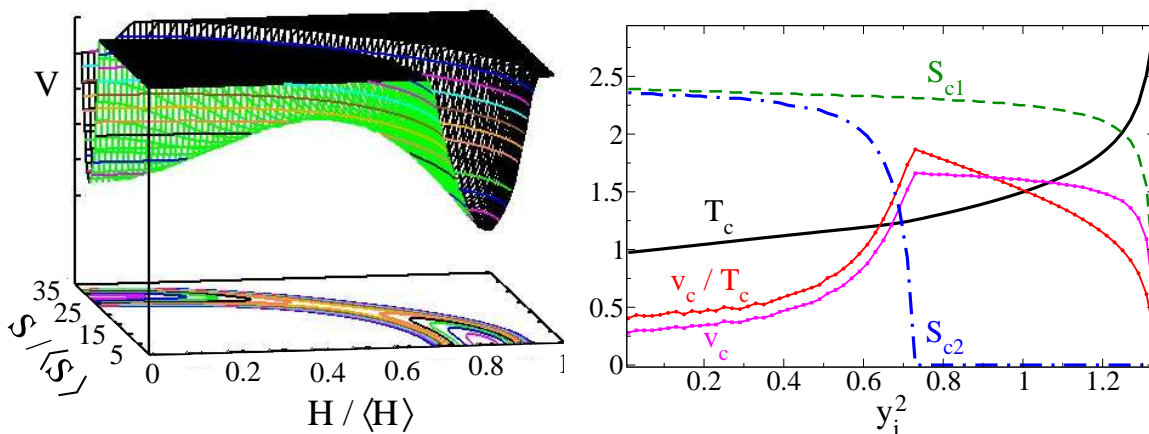
Figure 9. (a) Left: potential at critical temperature for typical point having smaller couplings: $\lambda_{\rm hs} = 0.633$, $\lambda_h = 0.633$, $\lambda_s = 0.167$, $y_i^2 = 1.25$, $\langle s \rangle = 10\,{\rm GeV}$. (b) Right: Dependences of T_c, v_c,
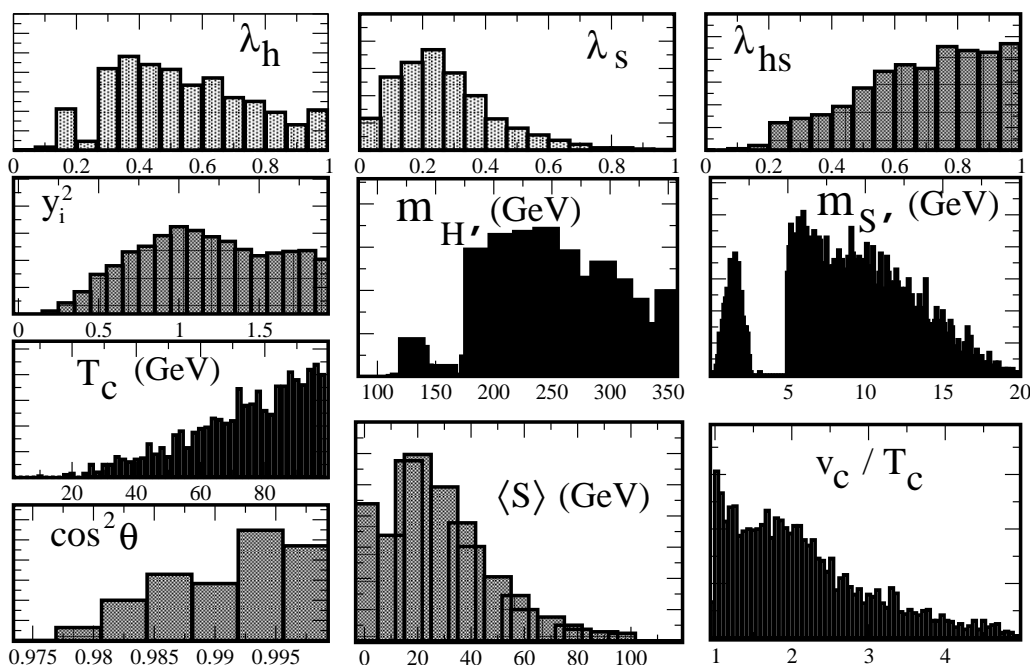

Figure 10. Distributions of accepted parameters with smaller values of the coupling constants, and $\lambda_{\rm hs} > 0$.

The dependence of the EWPT on the Yukawa coupling y_i^2 is due to the strong influence of y_i^2 on the S dynamics, which subsequently affects the dynamics of H through mixing. To understand this, we examined the dependences of various quantities, T_c, v_c, v_c/T_c, S_{c1}, and S_{c2} upon the Majorana Yukawa coupling y_i^2. An example is shown in figure 9(b). There is a notable rise in v_c associated with the decrease in S_{c2}—recall that this is the value of $\langle S \rangle$ in the EWSB vacuum at $T = T_c$; see figure 1. We can give an analytic explanation for the relation between v_c and S_{c2}. To this end, it is useful to think in terms

of an effective potential along the light direction H', which we approximate by the straight line paths connecting the symmetric and EWSB vacua shown in figure 1. At the critical temperature, we can write

$$\begin{pmatrix} H \\ S \end{pmatrix} = \begin{pmatrix} 0 \\ S_{c1} \end{pmatrix} + \begin{pmatrix} c_{\bar{\theta}} & s_{\bar{\theta}} \\ -s_{\bar{\theta}} & c_{\bar{\theta}} \end{pmatrix} \begin{pmatrix} H' \\ S' \end{pmatrix} \tag{3.9}$$

where the mixing angle $\bar{\theta}$ is generally different from the zero-temperature mixing angle θ. At $T = T_c$, the shape of the potential is roughly of the form $\lambda' H'^2 (H' - v'_c)^2 = \lambda H'^4 - 2g' H'^3 + \mu_c^2 H'^2$. From this form, we see that $v'_c = g'/\lambda'$. The cubic term can be estimated from the tree-level potential as

$$V_{\text{cubic}} = -2 s_{\bar{\theta}} \left(\lambda_{\text{hs}} c_{\bar{\theta}}^2 + 2\lambda_s s_{\bar{\theta}}^2 \right) S_{c1} H'^3 \quad \rightarrow \quad g' = s_{\bar{\theta}} \left(\lambda_{\text{hs}} c_{\bar{\theta}}^2 + 2\lambda_s s_{\bar{\theta}}^2 \right) S_{c1} \tag{3.10}$$

Similarly, the effective quartic coupling is $\lambda' = c_{\bar{\theta}}^4 \lambda_h + 2 c_{\bar{\theta}}^2 s_{\bar{\theta}}^2 \lambda_{\text{hs}} + s_{\bar{\theta}}^4 \lambda_s$. This gives the estimate

$$v_c \sim c_{\bar{\theta}} S_{c1} \frac{\left(s_{\bar{\theta}} c_{\bar{\theta}}^2 \lambda_{\text{hs}} + 2 s_{\bar{\theta}}^2 \lambda_s \right)}{\left(c_{\bar{\theta}}^4 \lambda_h + 2 c_{\bar{\theta}}^2 s_{\bar{\theta}}^2 \lambda_{\text{hs}} + s_{\bar{\theta}}^4 \lambda_s \right)} \tag{3.11}$$

From eq. (3.11) and figure 1 it is clear that for $\lambda_{\text{hs}} > 0$, a decrease in S_{c2} leads to an increase the mixing angle $\bar{\theta}$ and consequently an increase in v_c. This accounts for the initial growth in v_c for $y_i^2 \lesssim 0.6$ in figure 9. Beyond this point, S_{c2} remains constant, but S_{c1} decreases (hence $\bar{\theta}$ decreases), leading to a decrease in v_c. At the same time, eq. (3.4) shows that, for $\lambda_{\text{hs}} > 0$, decreasing S_{c1} leads to an increase in T_c. Both of the these effects cause v_c/T_c to go down with y_i^2 as observed in figure 9(b).

3.5 Constraints from electroweak precision observables

In refs. [14, 30] it was noted that electroweak precision observables provide a strong constraint on the related model containing a real singlet field. It is known that the oblique parameters S, T, U are best fit by a light Higgs boson, and this preference thus extends to singlets that mix with the doublet Higgs. The same constraints as for the real singlet apply to the Majoron model, since the extra Goldstone boson does not mix and therefore plays no role. We have thus carried out the same analysis as in [14, 30] to further constrain the accepted parameter sets described above. For completeness, the relevant formulas are given in appendix E. As a check on our implementation, we reproduced the results shown in figures 9 and 10 of [14].

The EWPO constraint indeed has a strong impact on the accepted parameter distributions. In our larger coupling sample, 730 out of 1000 points are removed for $\lambda_{\text{hs}} < 0$, and 1650 out of 1710 are excluded for $\lambda_{\text{hs}} > 0$; overall 88% of otherwise accepted points are thus ruled out, at 95% c.l. The resulting distributions are shown in figure 11. The most striking difference relative to the corresponding results without EWPO, figure 5, is the elimination of large values of the doublet-like mass $m_{H'}$, and the restriction to smaller mixing angles, $\cos^2 \theta \gtrsim 0.8$. There is also a stronger exclusion of small values of the Majorana Yukawa coupling.
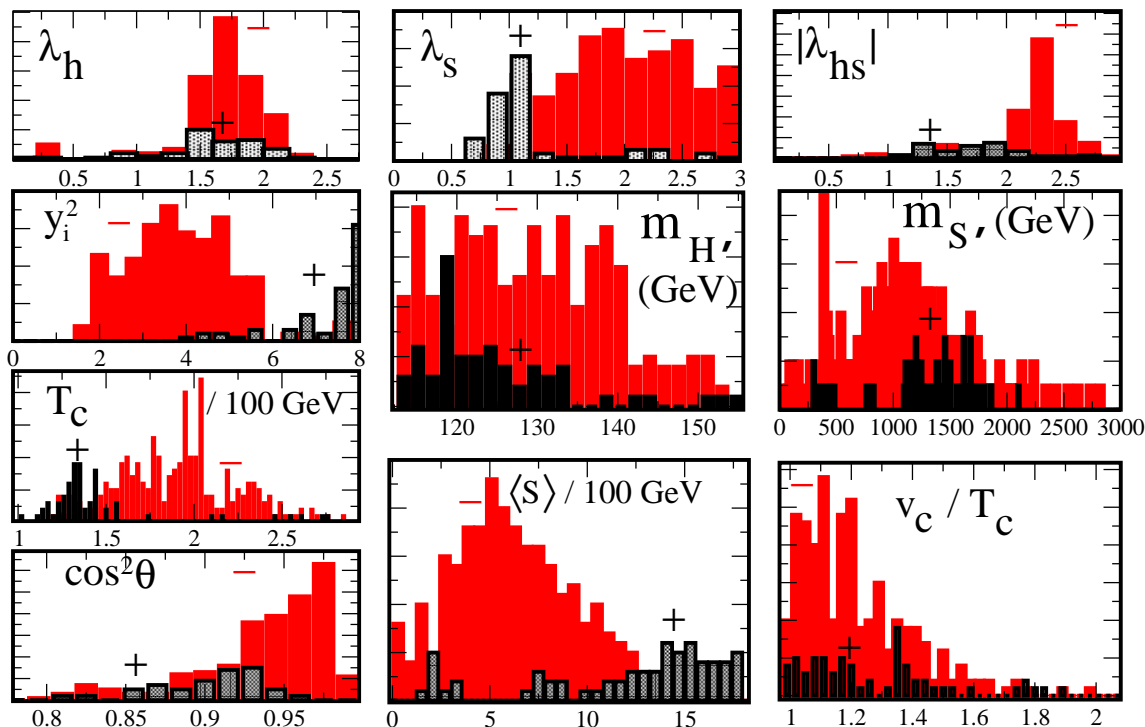
Figure 11. Distributions of accepted parameters with larger values of the coupling constants, after EWPO cut.

In the small-coupling sample, the EWPO constraint is even more powerful, eliminating 4370 out of 4860 parameter sets. Again, the effect is to eliminate higher values of the Higgs boson mass. The distributions are plotted in figure 12. The lower $m_{H'}$ values lead to correspondingly smaller values of the coupling λ_h.

Two cautionary remarks are, however, in order here. First, since the additional singlet can be light, a precision analysis of EWPO would require the inclusion of further parameters V, W, Z [31, 32]. Here, we do not go beyond S, T, U but leave an extensive EWPO analysis for future work. Second, the presence of additional new physics beyond the singlet-extension of the SM could considerably weaken the EWPO constraints. Therefore we refrain from imposing EWPO as a strict constraint in the following. Rather, we present results both with and without this constraint.

4 Implications for LHC

From the perspective of collider phenomenology, it is quite intriguing that all our accepted points feature a relatively light scalar, either the singlet- or the doublet-like state, with mass less than about 200 GeV. The other state is typically considerably heavier. Concerning detectability at the LHC, it is important to to know how the mass of the lighter state correlates with the mixing angle, i.e., how its couplings compare to those of a SM Higgs boson. To this purpose, figure 13 shows the scale factor ξ of the squared couplings versus mass of the lighter scalar. Specifically, $\xi = \cos^2\theta$ for the Higgs-like boson, while $\xi = \sin^2\theta$
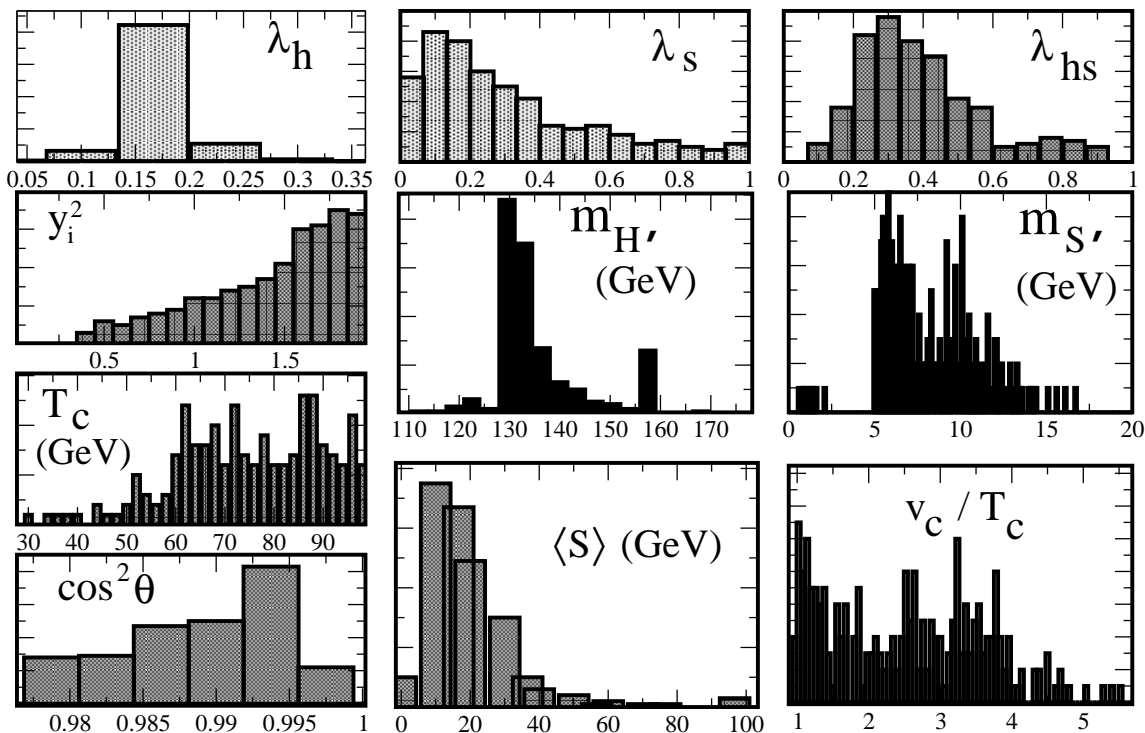
Figure 12. Distributions of accepted parameters with smaller values of the coupling constants, after EWPO cut.
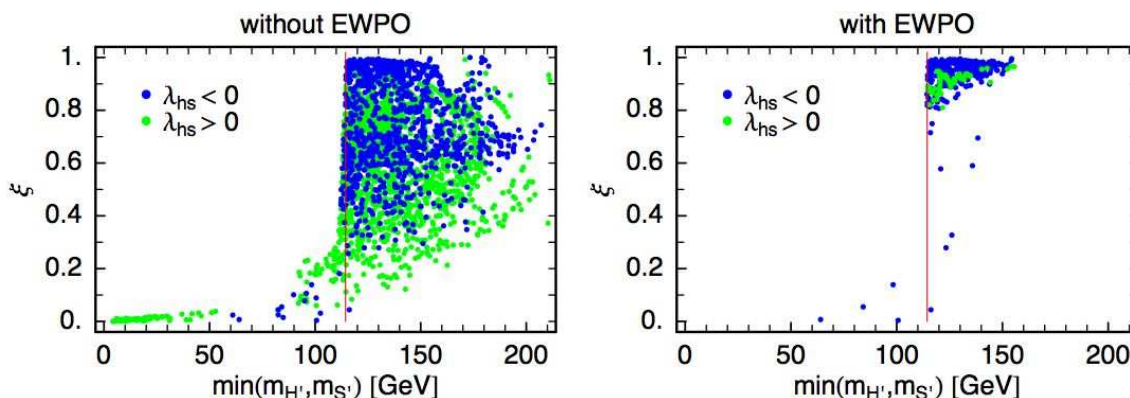

Figure 13. Distribution of scale factor of the squared couplings (relative to a SM Higgs) versus mass of the lighter scalar. For a doublet-like state $\xi = \cos^2\theta > 0.5$, while for a singlet-like state $\xi = \sin^2\theta < 0.5$. The vertical red line indicates the limit on a SM Higgs boson. The left (right) panel is without (with) the EWPO constraint.

for the singlet-like state. This can be compared with the LEP bound (figure 4) to get a feeling for how easily detectable the light boson may be at the LHC.

Let us first discuss the situation without the EWPO constraint, shown in the left plot of figure 13. The density of points in this scatter plot indicates that there would have been many examples providing a strong EWPT in the LEP-excluded region, but there is
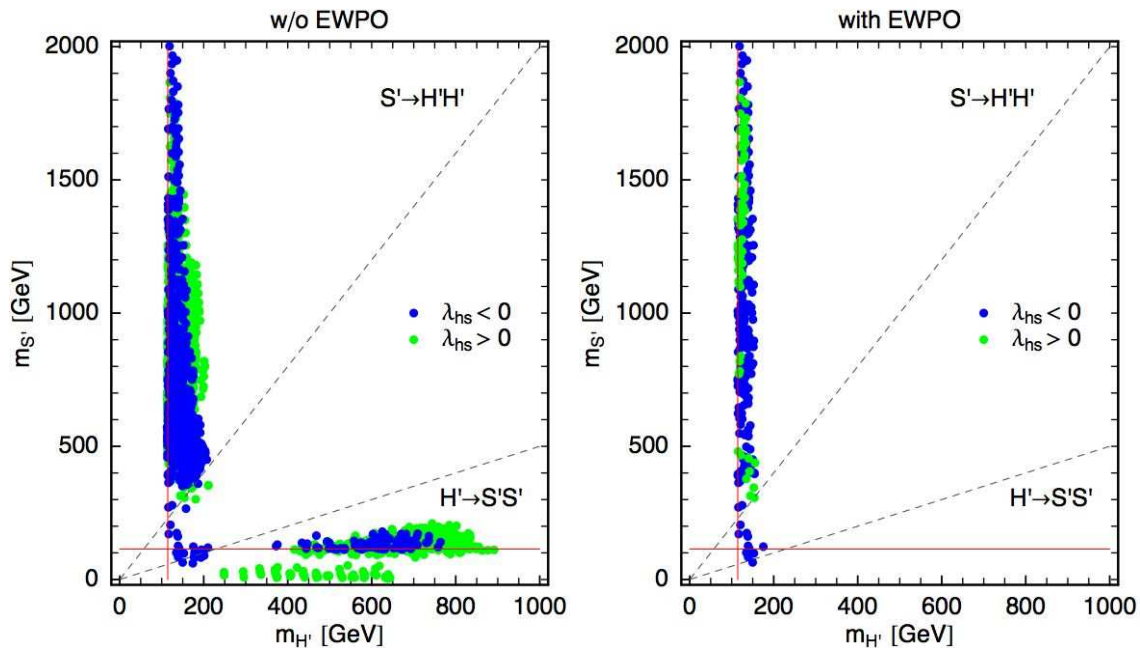
Figure 14. Scatter plots of the mostly-singlet versus mostly-doublet Higgs masses without (left) and with (right) EWPO constraint. The full red lines (horizontal and vertical) indicate the SM limit of $m_H^{\mathrm{SM}} > 114.4\,\mathrm{GeV}$. Above the upper dashed lines $S' \rightarrow H'H'$, below the lower dashed lines $H' \rightarrow S'S'$ is kinematically allowed.

not a strong bias toward being close to the limit. Nevertheless, there is an upper limit of $\min(m_{H'}, m_{S'}) \lesssim 200\,\mathrm{GeV}$ from the requirement of a strong EWPT (note also the lower limit on the mostly-doublet state of $m_{H'} \gtrsim 113\,\mathrm{GeV}$ from LEP data). Moreover, a large fraction of the accepted points features a sizable doublet-singlet mixing.

In the sample with small values of the couplings, the situation is different, because only small values of $m_S \lesssim 20\,\mathrm{GeV}$, and the mixing angle $\sin^2\theta \lesssim 0.02$, are present. This situation was considered for the similar model of a real singlet field in ref. [28]. There it was noted that values of $m_{S'} \lesssim 5\,\mathrm{GeV}$ (the B meson mass) are strongly constrained ($\theta < 10^{-2}$) by the decays $B \rightarrow S'X$ followed by $S' \rightarrow \mu^+\mu^-$. For $m_{S'}$ in the range $5\,\mathrm{GeV} \lesssim m_{S'} \lesssim 50\,\mathrm{GeV}$, the Higgs can decay into singlets, $H' \rightarrow S'S'$ at a level which can compete with the two photon final state, $H' \rightarrow \gamma\gamma$. For the accepted parameters in the small coupling regime, we find that the right-handed neutrinos are always heavier than $m_{S'}/2$. Therefore there is never an invisible decay channel $S' \rightarrow \nu_R\nu_R$ in this case. Instead, S' decays predominantly into $b\bar{b}$ quark pairs due to the small doublet-singlet mixing.

The situation changes quite drastically when applying the EWPO constraint, as shown in the right plot of figure 13. In this case, the allowed range shrinks to $\min(m_{H'}, m_{S'}) \lesssim 156\,\mathrm{GeV}$, and the regions with large mixing and/or a light singlet are almost completely cut away.

It is also useful to consider the correlation between the mostly-singlet and mostly-doublet Higgs masses, shown in figure 14, which reveals that typically one state is signifi-
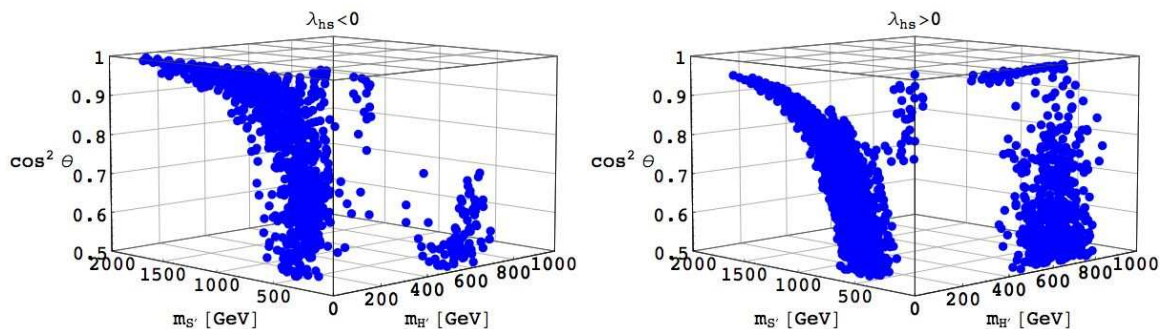
Figure 15. Triple correlation of mass eigenvalues and mixing angle for $\lambda_{\mathrm{hs}} < 0$ (left) and $\lambda_{\mathrm{hs}} > 0$ (right); without EWPO constraint.
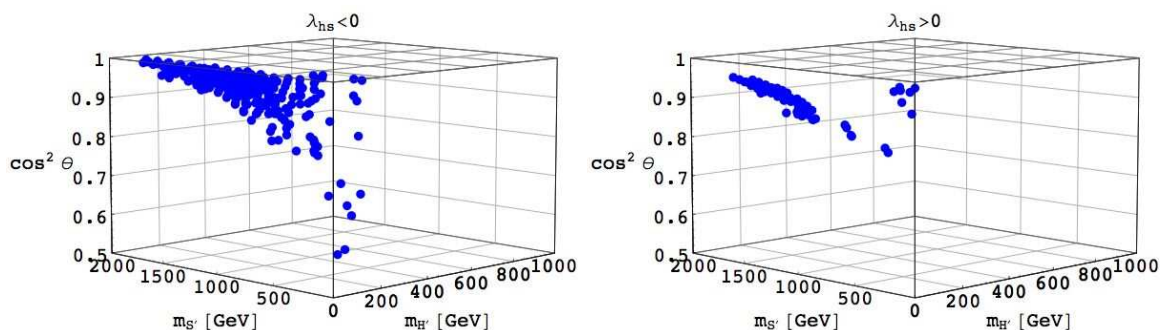

Figure 16. Same as figure 15 but with EWPO constraint applied.

cantly lighter than the other. For both, $\lambda_{\mathrm{hs}} < 0$ and $\lambda_{\mathrm{hs}} > 0$, we see distinct islands with either (i) $m_{H'} \lesssim 200\,\mathrm{GeV}$ and $m_{S'}$ ranging from few hundred GeV up to order TeV, or (ii) $m_{H'} > 200\,\mathrm{GeV}$ and a (much) lighter singlet. The latter region is, however, completely removed by the EWPO constraint. For $\lambda_{\mathrm{hs}} < 0$, there also exists a small region with $m_{H'} \sim 115 - 200\,\mathrm{GeV}$ and $m_{S'} \sim 50 - 130\,\mathrm{GeV}$. The triple correlation between the two masses and the mixing angle is shown in figures 15 and 16.

Regarding the decay modes, we see from figure 14 that for most points Higgs-to-Higgs decays, either $S' \to H'H'$ or $H' \to S'S'$, are allowed, which could modify the branching ratios relative to those of a SM Higgs boson. (If Higgs-to-Higgs decays are absent, the branching ratios of both the H' and the S' are just the same as those of a SM Higgs.) Denoting the lighter of the two states as h_1 and the heavier one as h_2, the generic expression for the decay width is

$$\Gamma(h_2 \to h_1 h_1) = \frac{g_{211}^2}{8\pi m_2}\sqrt{1 - 4m_1^2/m_2^2}\,, \tag{4.1}$$

where cubic coupling g_{211} is given by

$$g_{H'S'S'} = 24\lambda_h \langle h \rangle c_\theta s_\theta^2 - 24\lambda_s \langle s \rangle s_\theta c_\theta^2 + 4\lambda_{\mathrm{hs}} \left(\langle h \rangle c_\theta (c_\theta^2 - 2s_\theta^2) - \langle s \rangle s_\theta (s_\theta^2 - 2c_\theta^2) \right) \tag{4.2}$$

for $h_2 = H'$, $h_1 = S'$ and

$$g_{S'H'H'} = 24\lambda_h \langle h \rangle s_\theta c_\theta^2 + 24\lambda_s \langle s \rangle c_\theta s_\theta^2 + 4\lambda_{\mathrm{hs}} \left(\langle h \rangle s_\theta (s_\theta^2 - 2c_\theta^2) + \langle s \rangle c_\theta (c_\theta^2 - 2s_\theta^2) \right) \tag{4.3}$$

– 19 –

for $h_2 = S'$, $h_1 = H'$. Here, $c_\theta = \cos\theta$ and $s_\theta = \sin\theta$. The branching ratio is then given by

$$BR(h_2 \to h_1 h_1) = \frac{\Gamma(h_2 \to h_1 h_1)}{\xi\Gamma(H_{\mathrm{SM}}) + \Gamma(h_2 \to h_1 h_1)}\,, \tag{4.4}$$

where $\xi = \cos^2\theta \ (\sin^2\theta)$ for $h_2 = H' \ (S')$ and $\Gamma(H_{\mathrm{SM}})$ is the total decay width of the SM Higgs boson with same mass as h_2. We use HDECAY [35] to compute $\Gamma(H_{\mathrm{SM}})$. In the numerical analysis, we find that $S' \to H'H'$ decay typically has a rate of only a few percent, $BR(S' \to H'H') \lesssim 5\%$, and is therefore negligible over most of the parameter space.[4] For the mostly-doublet state, on the other hand, Higgs-to-Higgs decays can be important in the region $m_{H'} < 200\,\mathrm{GeV}$ and $m_{S'} \sim 50 - 100\,\mathrm{GeV}$. Our data set contains six points with $m_{H'} \sim 175 - 200\,\mathrm{GeV}$ and $m_{S'} \sim 60 - 95\,\mathrm{GeV}$ which have $BR(H' \to S'S') \sim 3 - 8\%$. With $\cos\theta \gtrsim 0.9$ these points have small doublet-singlet mixing. The singlet here decays 80–85% of the time to $b\bar{b}$ and about 9% to $\tau^+\tau^-$, leading to $4b$, $2b2\tau$ and 4τ final states. We also find one point with $m_{H'} = 150\,\mathrm{GeV}$, $m_{S'} = 64\,\mathrm{GeV}$, $\cos\theta = 0.99$ and $BR(H' \to S'S') = 56\%$. This point remains after EWPO contraints. It is also worthwhile to remember that, even when Higgs-to-Higgs decays are absent or negligible, the total decay width is modified by a factor $xi = \cos^2\theta \ (\sin^2\theta)$ in the case of H' (S'), relative to the SM Higgs boson.

Let us finally discuss the discovery potential at the LHC. To this end we use the CMS expectations on SM Higgs boson searches presented in [36]. Figure 10.38 of [36] shows the luminosity needed for a 5σ discovery in various standard search channels. For H' and S', this luminosity scales with $1/\xi^2$ due to the reduced production cross section, and, where applicable, a factor stemming from the modification of the branching ratios into SM particles; for the H':

$$\frac{BR(H' \to X_{\mathrm{SM}})}{BR(H_{\mathrm{SM}} \to X_{\mathrm{SM}})} = \frac{\xi\,\Gamma(H_{\mathrm{SM}})}{\xi\Gamma(H_{\mathrm{SM}}) + \Gamma(H' \to S'S')}\,, \tag{4.5}$$

with $\xi = \cos^2\theta$, and analogously for S' with $H' \leftrightarrow S'$ and $\xi = \sin^2\theta$. The resulting luminosity needed for a 5σ discovery is shown in figure 17; the left (right) plot shows the lighter (heavier) mass eigenstate. Blue dots represent a mostly-doublet Higgs, green dots a mostly-singlet one; points in darker colour are those which survive the EWPO constraints. The number and nature of Higgs bosons which are within discovery reach with 30 fb^{-1} of data is shown in figure 18.

In summary, we conclude that there is a strong discovery potential for this nonstandard Higgs sector, if it is the origin of a strong EWPT. This holds in particular for the mostly-doublet Higgs, but in many cases also for the mostly-singlet one. There are even a couple of points where both H' and S' could be discovered at the LHC with 30 fb^{-1} of integrated luminosity. With higher luminosity, the prospects for discovering both mass eigenstates are quite promising. The alert reader will note, however, that figure 17 is limited to $115\,\mathrm{GeV} \leq m_{H',S'} \leq 600\,\mathrm{GeV}$. In figure 18, we also show $m_{S'} < 115\,\mathrm{GeV}$, but the S' can be observed in this case. The reason is that the experimental analyses in [36] only cover

---

[4]The branching ratio of $S' \to H'H'$ is enhanced for $\cos\theta \to 1$, but in this case the S' production rate goes to zero. Our data set contains one point with $m_{S'} = 452\,\mathrm{GeV}$, $m_{H'} = 173\,\mathrm{GeV}$, $\cos\theta = 1$ and $BR(S' \to H'H') = 100\%$. All other points have $BR(S' \to H'H') \lesssim 5\%$.
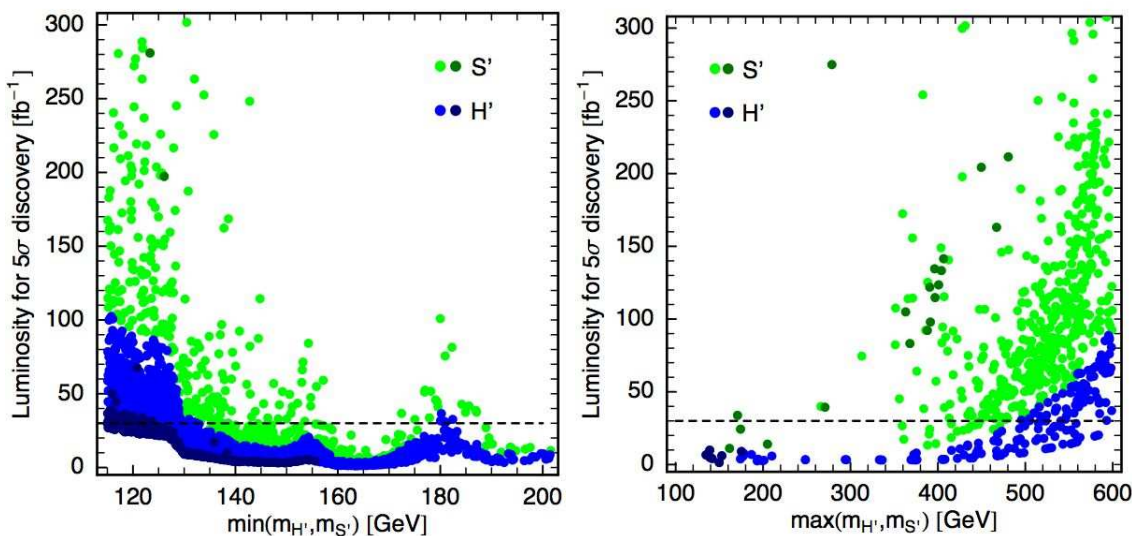
Figure 17. Luminosity needed for a 5σ discovery of the lighter (left plot) and the heavier (right plot) mass eigenstate, extrapolated from CMS results [36]. Blue dots represent a mostly-doublet Higgs, green dots a mostly-singlet one; points in darker colour survive EWPO constraints. The horizontal dashed lines indicate 30 fb^{-1} or three years of running at low luminosity.
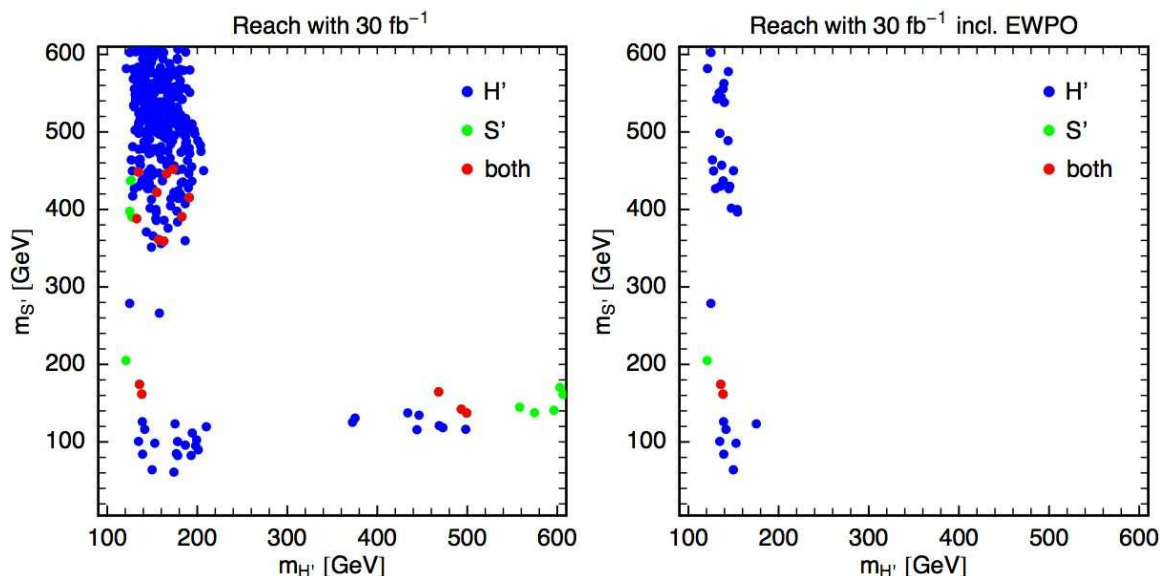

Figure 18. Discovery reach with 30 fb^{-1} in the $m_{S'}$ versus $m_{H'}$ plane. The different colours encode which state can be detected: blue stands for H', green for S', red for both. The left plot is without, the right one with EWPO constraints.

the mass range 115 GeV $\leq m_H \leq$ 600 GeV. In the majoron model, as well as in other singlet-extensions of the SM, it would however be interesting to search also for lighter and heavier states. We hope that the present work provides some motivation toward this end.

5 Conclusions

We have given an in-depth analysis of the EWPT in the singlet Majoron model at the one-loop level, taking account of the LEP constraints on the Higgs boson mass and mixing angle. Our broad scan of the model's parameter space indicates that a certain level of tuning is needed to get a strong enough transition for electroweak baryogenesis; many examples approximately satisfy the relation (3.7) which reduces the dimensionality of the parameter space. The zero-temperature one-loop correction was shown to play a crucial role in this respect, effectively reducing the negative mass squared of the Higgs and hence the critical temperature of the phase transition, to increase the figure of merit for the strength of the transition, v_c/T_c. These examples required rather large values of the coupling constants, as large as $\lambda_i \lesssim 3$. We also identified another population of accepted points with $\lambda_i \lesssim 1$ which has a different origin, and exists only for very small singlet masses $m_S \lesssim 20\,\text{GeV}$.

From the technical point of view, our job of identifying cases with a first order phase transition was made more difficult by the fact that both fields H and S usually evolve during the transition, so it is essential to keep track of both. Although numerous studies have been done on similar models with a singlet coupling to the Higgs, most of these assume that the singlet does not get a VEV, so this complication does not arise. Another difference is that a generic model of a real singlet interacting with H has many additional couplings which are odd in S, whereas the singlet Majoron model is constrained by the U(1) global lepton symmetry, which it spontaneously breaks. Due to the reduced number of coupling constants, we were able to make an exhaustive search of the parameter space. The singlet Majoron model also has the appeal of being theoretically motivated by the seesaw mechanism for neutrino masses. In our case, this must be supplemented by the requirement of small Dirac Yukawa couplings for the neutrinos, since we take the right-handed neutrinos to be lighter than the TeV scale.

Of course the strong phase transition is only interesting for baryogenesis if there is also a mechanism for producing the baryon asymmetry. Complex Majorana Yukawa couplings, which we assumed here to be real for simplicity, could provide the needed CP violation. Perhaps CP-violating reflections of the heavy neutrinos at the bubble walls could create a lepton asymmetry which would be converted to the baryon asymmetry via sphaleron interactions. This is a subject to which we hope to return.

It would be interesting to extend our study to the generation of gravitational waves. Although electroweak baryogenesis and gravity wave generation both need a "strong" phase transition, the criteria are different. In particular, relativistic bubble walls are favored for producing significant gravity waves. Ref. [33] has recently shown that this can be achieved in the related model of a real singlet with more general couplings (not respecting any Z_2 symmetry) than in the Majoron model.

Concerning collider phenomenology, we have shown that the LHC has a strong discovery potential for this nonstandard Higgs sector, if it is the origin of a strong EWPT. This includes the possibility of a SM-like Higgs boson with mass up to about $200\,\text{GeV}$, which has a sizeable branching fraction into a pair of light singlets. Moreover, with high enough luminosity there are good prospects to discover both the H' and the S' states. A dedicated experimental study would be worthwhile to cover masses below $115\,\text{GeV}$ and above $600\,\text{GeV}$.

Acknowledgments

A Analytic approximation for thermal potential

The method of smoothly matching the low- and high-T expansions for the one-loop thermal potential was given in ref. [5]. For convenience we repeat the formulas here. The nth order high-T (small M/T) expansion is given by [20]

$$
\begin{aligned}
V_{\mathrm{s,b}}(n) = & -\frac{\pi^2 T^4}{90} + \frac{M^2 T^2}{24} - \frac{M^3 T}{12\pi} - \frac{M^4}{64\pi^2}\left(\log\left(\frac{M^2}{T^2}\right) - c_b\right) \\
& + \frac{M^2 T^2}{2}\sum_{l=2}^{n}\left(\frac{-M^2}{4\pi^2 T^2}\right)^l \frac{(2l-3)!!\zeta(2l-1)}{(2l)!!(l+1)}, \qquad \text{bosons;} \\
V_{\mathrm{s,f}}(n) = & -\frac{7\pi^2 T^4}{720} + \frac{M^2 T^2}{48} + \frac{M^4}{64\pi^2}\left(\log\left(\frac{M^2}{T^2}\right) - c_f\right) \\
& - \frac{M^2 T^2}{2}\sum_{l=2}^{n}\left(\frac{-M^2}{4\pi^2 T^2}\right)^l \frac{(2l-3)!!\zeta(2l-1)}{(2l)!!(l+1)}\left(2^{2l-1} - 1\right), \qquad \text{fermions;} \\
& c_b = 3/2 + 2\log 4\pi - 2\gamma_E \cong 5.40762\,; \qquad c_f = c_b - 2\log 4 \cong 2.63503
\end{aligned}
\tag{A.1}
$$

respectively for bosons and fermions. The corresponding low-T (large M/T) expansion is [9]

$$
V_{\mathrm{l}}(n) = -e^{-M/T}\left(\frac{MT}{2\pi}\right)^{3/2} T \sum_{l=0}^{n} \frac{1}{2^l l!}\frac{\Gamma(5/2 + l)}{\Gamma(5/2 - l)}(T/M)^l.
\tag{A.2}
$$

By trial and error, one can find that the low- and high-T expansions can be smoothly matched onto each other using the approximation

$$
\begin{aligned}
V_b &= \Theta(x_b - (M/T)^2)\, V_{\mathrm{s,b}}(3) + \Theta((M/T)^2 - x_b)\left(V_{\mathrm{l}}(3) - \delta_b\, T^4\right) \\
V_f &= \Theta(x_f - (M/T)^2)\, V_{\mathrm{s,f}}(4) + \Theta((M/T)^2 - x_f)\left(V_{\mathrm{l}}(3) - \delta_f\, T^4\right)
\end{aligned}
\tag{A.3}
$$

where Θ is the step function with $x_b = 9.47134$ and $x_f = 5.47281$ for bosons and fermions, respectively. The small constant shifts of $V_{\mathrm{l}}(3)$ are made so that the function as well as its derivatives match at the transition point: $\delta_b = 3.19310 \times 10^{-4}$ and $\delta_f = 4.60156 \times 10^{-4}$. This gives an approximation with a relative error which is less than 0.5% for $M/T \to \infty$, and negligible for small M/T.

B Field dependent masses

Although it is convenient to express the potential and the field-dependent masses in terms of the complex VEV's, it is simpler to compute the masses in the real basis, where $H^0 = (h + i\phi_1)/\sqrt{2}$, $H^+ = (\phi_2 + i\phi_3)/\sqrt{2}$, $S = (s + ij)/\sqrt{2}$. We continue to express the field-dependent masses in terms of the complex fields, but assuming only h and s actually get VEV's: $H = h/\sqrt{2}$, $S = s/\sqrt{2}$.

The diagonal components of the zero-temperature scalar mass matrix, in the real basis h, ϕ_i, s, j, are

$$m_{h,h}^2 = \lambda_h \left(6|H|^2 - v_h^2\right) + \lambda_{\mathrm{hs}}|S|^2$$
$$m_{\phi_i,\phi_i}^2 = \lambda_h \left(2|H|^2 - v_h^2\right) + \lambda_{\mathrm{hs}}|S|^2$$
$$m_{s,s}^2 = \lambda_s \left(6|S|^2 - v_s^2\right) + \lambda_{\mathrm{hs}}|H|^2$$
$$m_{j,j}^2 = \lambda_s \left(2|S_2|^2 - v_s^2\right) + \lambda_{\mathrm{hs}}|H|^2 \tag{B.1}$$

Within the full 6×6 mass matrix, there is only one off-diagonal entry,

$$m_{s,h}^2 = m_{h,s}^2 = 2\lambda_{\mathrm{hs}}|H||S| \tag{B.2}$$

(Note that we can take H and S to be real here.) Thus one can analytically find all the field-dependent mass squared eigenvalues, by diagonalizing the h-s sector.

For the ring improvement, we must add thermal corrections to the mass squared matrix,

$$\delta m_H^2 = T^2 \left(\frac{1}{2}\lambda_h + \frac{1}{12}\lambda_{\mathrm{hs}} + \frac{1}{16}(3g^2 + g'^2) + \frac{1}{4}y_t^2\right) \tag{B.3}$$

$$\delta m_S^2 = T^2 \left(\frac{1}{3}\lambda_s + \frac{1}{6}\lambda_{\mathrm{hs}} + \frac{1}{24}\sum_i y_i^2\right) \tag{B.4}$$

They can be computed by inserting the zero-temperature masses into the high-T expansion of the one-loop thermal potential, and reading off the corrections to the mass terms (the coefficients of the terms quadratic in H and S). These thermal masses are the same for each real component (h, ϕ_i or s, j) within the H or S fields, respectively. Since $\delta m_H^2 \neq \delta m_S^2$, the thermal mass matrix has to be diagonalized independently of the zero-temperature mass matrix.

The field-dependent masses of the relevant fermions are given by

$$m_t^2 = y_t^2|H|^2, \quad m_{\nu_i}^2 = y_i^2|S|^2 \tag{B.5}$$

They do not need to be thermally corrected for the ring improvement. In the imaginary time formalism of finite-temperature field theory, where the effective squared masses of the Matsubara modes are $M^2(\phi, T) + (2\pi nT)^2$ for bosons and $M^2(\phi, T) + (2\pi(n + \frac{1}{2}T)^2$ for fermions. Only for the $n = 0$ modes of the bosons can there be an infrared divergence due to vanishing $M^2(\phi)$ which would make it important to include the perturbative $g^2 T^2$ contribution to M^2.

The only other fields we must consider are the gauge bosons. In the basis of $W_1, W_2,$ W_3, B, the mass matrix is

$$m^2_{\text{gauge}}(H, T) = \frac{|H^2|}{2} \begin{pmatrix} g^2 & & & \\ & g^2 & & \\ & & g^2 & gg' \\ & & gg' & g'^2 \end{pmatrix} + T^2 \begin{pmatrix} g^2 & & & \\ & g^2 & & \\ & & g^2 & \\ & & & g'^2 \end{pmatrix} \begin{cases} 2, \text{ longitudinal}; \\ 0, \text{ transverse}. \end{cases} \quad \text{(B.6)}$$

Only the longitudinal components get a thermal correction at leading order in the gauge couplings.

C Renormalization constants

To express the solutions to the renormalization conditions (2.5) it is convenient to define multiplicities g_i for the respective fields as: 1 for each real scalar, -12 for the top quark, -2 for each of the three right-handed neutrinos, 2 for each transverse gauge boson, 1 for longitudinal gauge bosons. It is straightforward to show that

$$\ln \mu^2 = \frac{\sum_i g_i m_i^2 \frac{\partial m_i^2}{\partial S} \left(\ln m_i^2 - 1 \right)}{\sum_i g_i m_i^2 \frac{\partial m_i^2}{\partial S}} \quad \text{(C.1)}$$

$$A = -\frac{1}{32\pi^2 \langle H \rangle} \sum_i g_i m_i^2 \frac{\partial m_i^2}{\partial H} \left(\ln \frac{m_i^2}{\mu^2} - 1 \right) \quad \text{(C.2)}$$

evaluated at the minimum of the tree level potential. These conditions ensure that the position of this minimum remains unchanged at one loop.

D Beta functions

Defining $\beta_\lambda = 16\pi^2 d\lambda/d\ln \mu^2$, the beta functions for the largest couplings in the singlet Majoron model are [34]

$$\beta_{\lambda_h} = 12\lambda_h^2 + \frac{1}{2}\lambda_{\text{hs}}^2 + \frac{9}{4}g^4 + \frac{9}{8}(g^2 + g'^2)^2 - 3y_t^4$$
$$+ \lambda_h \left(-\frac{9}{2}g^2 - \frac{3}{2}g'^2 + 6y_t^2 \right) \quad \text{(D.1)}$$

$$\beta_{\lambda_{\text{hs}}} = 6\lambda_h \lambda_{\text{hs}} + 2\lambda_{\text{hs}}^2 + 4\lambda_{\text{hs}}\lambda_s + \lambda_{\text{hs}} \left(-\frac{9}{4}g^2 - \frac{3}{4}g'^2 + 3y_t^2 + \frac{1}{2}\sum y_i^2 \right) \quad \text{(D.2)}$$

$$\beta_{\lambda_s} = 2\lambda_{\text{hs}}\lambda_s + 10\lambda_s^2 - \frac{1}{2}\sum y_i^4 + \lambda_s \sum y_i^2 \quad \text{(D.3)}$$

$$\beta_y = \frac{3}{4}y_t^3 + \frac{1}{2}y_t \left(3y_t^2 - \frac{5}{12}g'^2 - \frac{9}{4}g^2 - 8g_s^2 \right) \quad \text{(D.4)}$$

$$\beta_{y_j} = \frac{1}{8}y_j^3 + \frac{1}{4}y_j \sum y_i^2 \quad \text{(D.5)}$$

We integrate these starting from the scale $\mu =$100 GeV up to the first Landau pole (where any of the running couplings diverge), taking 3 generations of right-handed neutrinos. The running of the gauge couplings is neglected in this estimate.

E   Electroweak precision observables

To evaluate the impact of constraints on the oblique parameters S, T, U, we follow the procedure of references [14, 30], defining $\Delta\chi^2$ as in eq. (5.4) of [14], and taking points with $\Delta\chi^2 > 7.8$ to be excluded at 95% c.l. Explicit expressions for T were given in those references, but not for S or U. These can be derived from the definitions found in eqs. (10.61) of the PDG Review of Particle Properties [37], and the expressions for the W and Z self-energies in appendix A of [30]. We find that the contribution to S from the Higgs sector is

$$
\begin{aligned}
-2\pi S_{\text{new}} = \cos^2\theta & \left(\frac{1}{m_Z^2} \left[G(H', Z) - m_{H'}^2 F_1(Z, H', Z) \right] + F_2(H', Z, Z) \right. \\
& \left. + 2 \left[F_0(W, H', 0) - F_0(W, H', W) + F_0(Z, H', Z) - F_0(Z, H', 0) \right] \right) \\
& + \sin^2\theta \left(H' \to S' \right)
\end{aligned}
\tag{E.1}
$$

where

$$
G(a, b) = \frac{1}{4}\left(m_a^2 + m_b^2\right) - \frac{m_a^2 m_b^2}{2(m_a^2 - m_b^2)} \ln\frac{m_a^2}{m_b^2} - \frac{1}{2}\left(m_a^2 \ln m_a^2 + m_b^2 \ln m_b^2\right) \tag{E.2}
$$

$$
F_n(a, b, c) = \int_0^1 dx\, x^n \ln((1-x)m_a^2 + + x\, m_b^2 - x(1-x)m_c^2) \tag{E.3}
$$

and we define $m_0^2 \equiv 0$. The deviation from the standard model prediction is obtained by taking

$$
\Delta S = S_{\text{new}} - S_{\text{new}}(\phi = 0,\, m_{H'}^2 = m_{S'}^2 = m_h^2) \tag{E.4}
$$

Similarly, U can be inferred from the combination

$$
\begin{aligned}
2\pi(S_{\text{new}} + U_{\text{new}}) = \cos^2\theta & \left(\frac{m_{H'}^2}{m_W^2} \left[F_1(W, H', 0) - F_1(W, H', Z, W) \right] + F(H', W, 0) \right. \\
& \left. + 2\left[F_0(W, H', W) - F_0(W, H', 0) \right] + F_1(H', W, 0) - F_1(H', W, W) \right) \\
& + \sin^2\theta \left(H' \to S' \right)
\end{aligned}
\tag{E.5}
$$

where $F = F_1 - F_2$. ΔU is computed analogously to (E.4).

References

[1] K. Kajantie, M. Laine, K. Rummukainen and M.E. Shaposhnikov, *Is there a hot electroweak phase transition at $m_H \gtrsim m_W$?*, *Phys. Rev. Lett.* **77** (1996) 2887 [hep-ph/9605288] [SPIRES].

[2] R. Apreda, M. Maggiore, A. Nicolis and A. Riotto, *Supersymmetric phase transitions and gravitational waves at LISA*, *Class. Quant. Grav.* **18** (2001) L155 [hep-ph/0102140] [SPIRES]; *Gravitational waves from electroweak phase transitions*, *Nucl. Phys.* **B 631** (2002) 342 [gr-qc/0107033] [SPIRES];

C. Grojean and G. Servant, *Gravitational Waves from Phase Transitions at the Electroweak Scale and Beyond*, *Phys. Rev.* **D 75** (2007) 043507 [`hep-ph/0607107`] [SPIRES];
S.J. Huber and T. Konstandin, *Production of Gravitational Waves in the NMSSM*, *JCAP* **05** (2008) 017 [`arXiv:0709.2091`] [SPIRES].

[3] M.S. Turner and L.M. Widrow, *Inflation Produced, Large Scale Magnetic Fields*, *Phys. Rev.* **D 37** (1988) 2743 [SPIRES];
G. Baym, D. Bödeker and L.D. McLerran, *Magnetic fields produced by phase transition bubbles in the electroweak phase transition*, *Phys. Rev.* **D 53** (1996) 662 [`hep-ph/9507429`] [SPIRES].

[4] J.R. Espinosa, M. Quirós and F. Zwirner, *On the electroweak phase transition in the minimal supersymmetric Standard Model*, *Phys. Lett.* **B 307** (1993) 106 [`hep-ph/9303317`] [SPIRES];
M.S. Carena, M. Quirós and C.E.M. Wagner, *Opening the Window for Electroweak Baryogenesis*, *Phys. Lett.* **B 380** (1996) 81 [`hep-ph/9603420`] [SPIRES];
J.M. Cline and K. Kainulainen, *Supersymmetric Electroweak Phase Transition: beyond Perturbation Theory*, *Nucl. Phys.* **B 482** (1996) 73 [`hep-ph/9605235`] [SPIRES];
M. Laine, *Effective theories of MSSM at high temperature*, *Nucl. Phys.* **B 481** (1996) 43 [*Erratum ibid.* **B 548** (1999) 637] [`hep-ph/9605283`] [SPIRES];
G.R. Farrar and M. Losada, *SUSY and the electroweak phase transition*, *Phys. Lett.* **B 406** (1997) 60 [`hep-ph/9612346`] [SPIRES];
B. de Carlos and J.R. Espinosa, *The baryogenesis window in the MSSM*, *Nucl. Phys.* **B 503** (1997) 24 [`hep-ph/9703212`] [SPIRES];
J.M. Cline and K. Kainulainen, *Supersymmetric electroweak phase transition: dimensional reduction versus effective potential*, *Nucl. Phys.* **B 510** (1998) 88 [`hep-ph/9705201`] [SPIRES];
M. Laine and K. Rummukainen, *A strong electroweak phase transition up to $m_H \sim 105\,GeV$*, *Phys. Rev. Lett.* **80** (1998) 5259 [`hep-ph/9804255`] [SPIRES]; *The MSSM electroweak phase transition on the lattice*, *Nucl. Phys.* **B 535** (1998) 423 [`hep-lat/9804019`] [SPIRES];
M. Losada, *The two-loop finite-temperature effective potential of the MSSM and baryogenesis*, *Nucl. Phys.* **B 537** (1999) 3 [`hep-ph/9806519`] [SPIRES];
S.J. Huber and M.G. Schmidt, *SUSY variants of the electroweak phase transition*, *Eur. Phys. J.* **C 10** (1999) 473 [`hep-ph/9809506`] [SPIRES]; *Electroweak baryogenesis: concrete in a SUSY model with a gauge singlet*, *Nucl. Phys.* **B 606** (2001) 183 [`hep-ph/0003122`] [SPIRES].

[5] J.M. Cline and P.-A. Lemieux, *Electroweak phase transition in two Higgs doublet models*, *Phys. Rev.* **D 55** (1997) 3873 [`hep-ph/9609240`] [SPIRES].

[6] M. Laine and K. Rummukainen, *Two Higgs doublet dynamics at the electroweak phase transition: a non-perturbative study*, *Nucl. Phys.* **B 597** (2001) 23 [`hep-lat/0009025`] [SPIRES];
L. Fromme, S.J. Huber and M. Seniuch, *Baryogenesis in the two-Higgs doublet model*, *JHEP* **11** (2006) 038 [`hep-ph/0605242`] [SPIRES].

[7] Y. Kikukawa, M. Kohda and J. Yasuda, *First-order restoration of $SU(N_f) \times SU(N_f)$ chiral symmetry with large N_f and Electroweak phase transition*, *Phys. Rev.* **D 77** (2008) 015014 [`arXiv:0709.2221`] [SPIRES]; *The strongly coupled fourth family and a first-order electroweak phase transition. I. Quark sector*, `arXiv:0901.1962` [SPIRES];
J.M. Cline, M. Jarvinen and F. Sannino, *The Electroweak Phase Transition in Nearly Conformal Technicolor*, *Phys. Rev.* **D 78** (2008) 075027 [`arXiv:0808.1512`] [SPIRES].

[8] C. Grojean, G. Servant and J.D. Wells, *First-order electroweak phase transition in the standard model with a low cutoff*, *Phys. Rev.* **D 71** (2005) 036001 [hep-ph/0407019] [SPIRES];
S.W. Ham and S.K. Oh, *Electroweak phase transition in the standard model with a dimension-six Higgs operator at one-loop level*, *Phys. Rev.* **D 70** (2004) 093007 [hep-ph/0408324] [SPIRES].

[9] G.W. Anderson and L.J. Hall, *The Electroweak phase transition and baryogenesis*, *Phys. Rev.* **D 45** (1992) 2685 [SPIRES].

[10] J.R. Espinosa and M. Quirós, *The Electroweak phase transition with a singlet*, *Phys. Lett.* **B 305** (1993) 98 [hep-ph/9301285] [SPIRES].

[11] J. Choi and R.R. Volkas, *Real Higgs singlet and the electroweak phase transition in the standard model*, *Phys. Lett.* **B 317** (1993) 385 [hep-ph/9308234] [SPIRES].

[12] S.W. Ham, Y.S. Jeong and S.K. Oh, *Electroweak phase transition in an extension of the standard model with a real Higgs singlet*, *J. Phys.* **G 31** (2005) 857 [hep-ph/0411352] [SPIRES].

[13] A. Ahriche, *What is the Criterion for a Strong First Order Electroweak Phase Transition in Singlet Models?*, *Phys. Rev.* **D 75** (2007) 083522 [hep-ph/0701192] [SPIRES].

[14] S. Profumo, M.J. Ramsey-Musolf and G. Shaughnessy, *Singlet Higgs Phenomenology and the Electroweak Phase Transition*, *JHEP* **08** (2007) 010 [arXiv:0705.2425] [SPIRES].

[15] V. Barger, P. Langacker, M. McCaskey, M. Ramsey-Musolf and G. Shaughnessy, *Complex Singlet Extension of the Standard Model*, *Phys. Rev.* **D 79** (2009) 015018 [arXiv:0811.0393] [SPIRES].

[16] A. Ashoorioon and T. Konstandin, *Strong electroweak phase transitions without collider traces*, arXiv:0904.0353 [SPIRES].

[17] K. Enqvist, K. Kainulainen and I. Vilja, *Phase transitions in the singlet majoron model*, *Nucl. Phys.* **B 403** (1993) 749 [SPIRES];
Y. Kondo, I. Umemura and K. Yamamoto, *First order phase transition in the singlet Majoron model*, *Phys. Lett.* **B 263** (1991) 93 [SPIRES];
N. Sei, I. Umemura and K. Yamamoto, *Constraints on the electroweak phase transition in the singlet majoron model*, *Phys. Lett.* **B 299** (1993) 286 [SPIRES].

[18] Y. Chikashige, R.N. Mohapatra and R.D. Peccei, *Are There Real Goldstone Bosons Associated with Broken Lepton Number?*, *Phys. Lett.* **B 98** (1981) 265 [SPIRES].

[19] J.M. Cline, K. Kainulainen and S. Paban, *Stability of neutrinos in the singlet majoron model*, *Phys. Lett.* **B 319** (1993) 513 [hep-ph/9309316] [SPIRES].

[20] P. Arnold and O. Espinosa, *The Effective potential and first order phase transitions: beyond leading-order*, *Phys. Rev.* **D 47** (1993) 3546 [*Erratum ibid.* **D 50** (1994) 6662] [hep-ph/9212235] [SPIRES].

[21] R.R. Parwani, *Resummation in a hot scalar field theory*, *Phys. Rev.* **D 45** (1992) 4695 [*Erratum ibid.* **D 48** (1993) 5965] [hep-ph/9204216] [SPIRES].

[22] D. Comelli and J.R. Espinosa, *Bosonic thermal masses in supersymmetry*, *Phys. Rev.* **D 55** (1997) 6253 [hep-ph/9606438] [SPIRES].

[23] M.E. Shaposhnikov, *Possible Appearance of the Baryon Asymmetry of the Universe in an Electroweak Theory*, *JETP Lett.* **44** (1986) 465 [*Pisma Zh. Eksp. Teor. Fiz.* **44** (1986) 364] [SPIRES]; *Baryon Asymmetry of the Universe in Standard Electroweak Theory*, *Nucl. Phys.* **B 287** (1987) 757 [SPIRES].

[24] J.M. Cline, *Baryogenesis*, lectures given at *Les Houches Summer School — Session 86: Particle Physics and Cosmology: The Fabric of Spacetime*, Les Houches, France, July 31 – August 25 2006, hep-ph/0609145 [SPIRES].

[25] ALEPH collaboration, DELPHI collaboration, L3 collaboration, OPAL collaboration, LEP Working Group for Higgs Boson Searches, S. Schael et al., *Search for neutral MSSM Higgs bosons at LEP*, *Eur. Phys. J.* **C 47** (2006) 547 [hep-ex/0602042] [SPIRES].

[26] A. Datta and A. Raychaudhuri, *Next to minimal Higgs: mass bounds and search prospects*, *Phys. Rev.* **D 57** (1998) 2940 [hep-ph/9708444] [SPIRES]; O. Bahat-Treidel, Y. Grossman and Y. Rozen, *Hiding the Higgs at the LHC*, *JHEP* **05** (2007) 022 [hep-ph/0611162] [SPIRES].

[27] CDF collaboration, D0 collaboration, *Combined CDF and DZero Upper Limits on Standard Model Higgs-Boson Production with up to 4.2 fb-1 of Data*, arXiv:0903.4001 [SPIRES].

[28] D. O'Connell, M.J. Ramsey-Musolf and M.B. Wise, *Minimal Extension of the Standard Model Scalar Sector*, *Phys. Rev.* **D 75** (2007) 037701 [hep-ph/0611014] [SPIRES].

[29] M.S. Carena, A. Megevand, M. Quirós and C.E.M. Wagner, *Electroweak baryogenesis and new TeV fermions*, *Nucl. Phys.* **B 716** (2005) 319 [hep-ph/0410352] [SPIRES].

[30] V. Barger, P. Langacker, M. McCaskey, M.J. Ramsey-Musolf and G. Shaughnessy, *LHC Phenomenology of an Extended Standard Model with a Real Scalar Singlet*, *Phys. Rev.* **D 77** (2008) 035005 [arXiv:0706.4311] [SPIRES].

[31] I. Maksymyk, C.P. Burgess and D. London, *Beyond S, T and U*, *Phys. Rev.* **D 50** (1994) 529 [hep-ph/9306267] [SPIRES].

[32] C.P. Burgess, S. Godfrey, H. Konig, D. London and I. Maksymyk, *A Global fit to extended oblique parameters*, *Phys. Lett.* **B 326** (1994) 276 [hep-ph/9307337] [SPIRES].

[33] D. Bödeker and G.D. Moore, *Can electroweak bubble walls run away?*, *JCAP* **05** (2009) 009 [arXiv:0903.4099] [SPIRES].

[34] G.D. Moore, private communication.

[35] A. Djouadi, J. Kalinowski and M. Spira, *HDECAY: a program for Higgs boson decays in the standard model and its supersymmetric extension*, *Comput. Phys. Commun.* **108** (1998) 56 [hep-ph/9704448] [SPIRES].

[36] CMS collaboration, G.L. Bayatian et al., *CMS technical design report, volume II: physics performance*, *J. Phys.* **G 34** (2007) 995 [SPIRES].

[37] PARTICLE DATA GROUP collaboration, C. Amsler et al., *Review of particle physics*, *Phys. Lett.* **B 667** (2008) 1 [SPIRES].